# GEOKINEMATICS OF CENTRAL EUROPE: NEW INSIGHTS FROM THE CERGOP-2/ENVIRONMENT PROJECT

**A.Caporali[1)], M. Becker[2)], I. Fejes[3,4)], L. Gerhatova[6)], D. Ghitau[5)], G. Grenerczy[3,4)], J. Hefty[6)], D. Medac[12)], G. Milev[7)], M. Mojzes[6)], M. Mulic[8)], A. Nardo[1)], P. Pesec[9)], T. Rus[5)], J. Simek[10)], J. Sledzinski[11)], M. Solaric[12)], G. Stangl[13)] , F. Vespe[14)], G. Virag[3)], F. Vodopivec[15)], F. Zablotskyi[16)]**

1) **Department of Geology, Paleontology and Geophysics, University of Padova, Italy**
2) **Institut für Physikalische Geodäsie, Technische Universität Darmstadt, Germany**
3) **Institute of Geodesy, Cartography and Remote Sensing, Satellite Geodetic Observatory, Penc, Hungary**
4) **MTA Research Group for Physical Geodesy and Geodynamics, Budapest, Hungary**
5) **Technical University of Civil engineering, Bucharest, Romania**
6) **Department of Theoretical Geodesy, Slovak University of Technology, Bratislava, Slovakia**
7) **Central Laboratory of Geodesy, Bulgarian Academy of Sciences, Sofia, Bulgaria**
8) **Department of Geodesy, Faculty of Civil Engineering, University of Sarajevo, Bosnia Herzegovina**
9) **Space Research Institute, Austrian Academy of Sciences, Graz, Austria**
10) **Research Institute on Geodesy, Topography and Cartography, Zdiby, Czech Republic**
11) **Institute of Geodesy and Geodetic Astronomy, Warsaw University of Technology, Poland**
12) **Faculty of Geodesy, University of Zagreb, Croatia**
13) **Federal Office of Metrology and Surveying, Graz, Austria**
14) **Centro di Geodesia Spaziale, Colombo, Agenzia Spaziale Italiana, Matera, Italy**
15) **Faculty of Civil and Geodetic Engineering, University of Ljubljana, Slovenia**
16) **Chair of Geodesy and Astronomy, Lviv Polytechnic National University, Ukraine**

**Keywords: GPS Geodesy, Central European Geodynamics, Central European Tectonics, Stress and Strain in Central Europe**

## Abstract

**The CERGOP2 project funded by the European Union from 2003 to 2006 under the 5th Framework Programme benefits from repeated measurements of the coordinates of epoch and permanent GPS stations forming the CEGRN network in Central Europe, starting 1994. We report on the results of the systematic processing of the available data up to 2005. The analysis work has yielded the velocities of some 60 sites, covering a variety of Central European tectonic provinces, from the Adria indenter to the Tauern window, the Pannonian basin, the Vrancea Seismic Zone and the Carpathian Mountains. The estimated velocities define kinematical patterns which outline, with varying spatial resolution depending on the station density and history, the present day tectonic flow in Central Europe. The CEGRN data show that the majority of active contraction originating from the Eurasia Nubia plate boundary and the microplate between them is taken up primarily in the Eastern Alps, the Dinarides, and the Pannonian Basin. After removal from the ITRF2000 velocities of a rigid rotation accounting for the mean motion of stable Europe, the residual velocities have random orientations with 0.3 mm/yr scatter. This low figure provides an upper estimate for the level of rigidity of the European Platform. A 2.3 mm/yr north-south oriented convergence rate is implied by our data between Adria and the Southern Alps, and a narrow -~60 km wide- contraction zone in the Southern Alps is identified, consistently with earlier results. An eastward extrusion north of the contraction zone corresponds with the extension of the Tauern Window. In the southeastern boundary of the microplate, 4-4.5 mm/yr motion of Adria decreases to ~1 mm/yr through the microplate, its boundary, and the Dinarides mountain range towards the southwestern part of the Pannonian Basin. Our data suggest that if the Pannonian Basin is subject to deformation, then it is most likely to be compressional than extensional. We conclude that compression and associated contraction due to the Adria collision with the Alps and the Dinarides is likely to fade away in the Western and Northern Carpathians, where our velocities and strain rates show no significant deformation.**

## 1. Introduction

**The Central European GPS Geodynamic Reference Network (CEGRN) was established in 1994 (Barlik et al., 1994), and extensively measured through cooperative effort by Central European research groups under the Central European Geodynamics Research Projects (CERGOP). CERGOP was supported by the European Union in 1995-98. To ensure the long time scale maintenance of CEGRN, a consortium of 14 research groups from 13 Central European Countries was formed in 2001 (Fejes, 2006). Based on this CEGRN Consortium a new phase of the project, called CERGOP-2/Environment, again sponsored by the European Union, was carried out in 2003-2006. The CERGOP-2/Environment project activities ranged from data and site validation, processing of GPS data, reference frame and time series computation, velocities and strain rates, zenith tropospheric delay and evaluation of the results with the aim to improve the understanding of geokinematics in Central Europe. This paper summarizes the basic achievements of a three year work which, in turn, has capitalized on, and extended the work of nearly one decade before. To support this multinational coordinated activity, a rather structured organization has been set up among the contributing research groups, to ensure proper harmonization of vertical and horizontal geodetic measurements. The horizontal and vertical patterns of velocities which result from the observations define four domains of active deformation: the Adriatic indenter, the Eastern Alps, the European Foreland and the Pannonian basin with the Western Carpathians. We report evidence of convergence between the Adria indenter and the stable European foreland, with the Tauern window in the Eastern Alps interacting with the Pannonian basin. The Carpathians have an history of erosion and uplift that could imply a pattern of horizontal and vertical intraplate velocities. We shall see however that the estimated velocities are consistent with a rigidly rotating Eurasia, ruling out significant intraplate deformations in this area.**

**This paper is organized in seven sections. In section 2 we review the tectonic features of Central Europe, and particularly the existing information on the kinematical evolution, properties of the crust/lithosphere, heat flow, and the stress field which is**

**inferred from a combination of geophysical data, such as fault plane solutions and in situ stress measurements. In section 3 we review our data base, which consists of raw GPS data from campaign and permanent sites, and the auxiliary information (logsheets, calibration tables and similar) which are necessary to validate the data to be processed. Section 4 is devoted to exemplify some local issues which may affect the coordinates and hence the velocities: electromagnetic interference, effects in the coordinates of the improvement of models of the phase center for specific antennas, and multipath are presented as examples of the tests done to understand the dependency of the computed coordinates on technical and environmental aspects. Section 5 addresses the estimate of velocities for campaign and permanent GPS stations of CEGRN by normal equation stacking, the alignment of the realization of the reference frame to the internationally adopted ITRF2000. Finally, the interpolation of velocities to a regular grid is done by least squares collocation, to highlight specific patterns while keeping track of interpolation and random errors. Section 6 is devoted to the analysis of stability of the time series of those permanent stations involved in the project and used for reference frame purposes. The removal of periodic terms, the noise characterization in time and frequency domain and the estimate of the stability of the time series in the sense of Allan variance are exemplified, with the intent to prove that the selection of reference sites for datum definition has been addressed with the maximum care, and that the selected stations are in fact best suited to define a Central European Reference Frame properly aligned to the ITRF2000. Section 7 summarizes the velocity gradient information obtained from the estimated velocities: the velocity gradient is resolved into an isotropic part (extension or dilatation), eigenvectors and their orientation. The map of the strain rate for Central Europe is presented as a geodetic counterpart of the stress map available from independent geophysical data. Section 8 summarizes the impact of the estimated velocities and velocity gradients on our understanding of the recent evolution of surface deformation in Central Europe.**

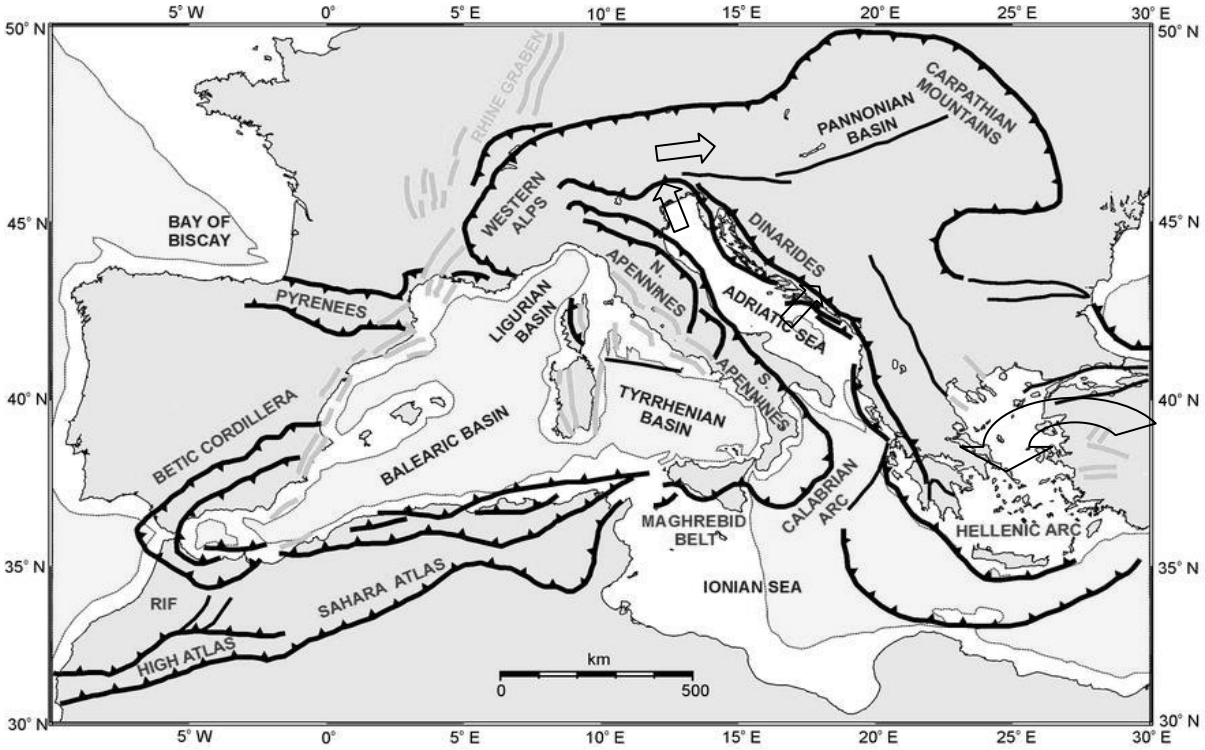


***Fig. 1. Structural setting of Continental Europe, the Mediterranean and the Hellenic arc, adapted from Jolivet and Faccenna (2000). Arrows qualitatively indicate the expected direction of the most important kinematic units in the study area.***

## 2. Tectonic structure

## 2.1 Kinematics

**The tectonic history of the Carpathian-Pannonian system is dominated by plate interactions to the south (Fig.1). The break up of Pangea in the early Mesozoic created the Tethys Ocean and an irregular continental margin across what was then southern Europe. This rifting also produced a collage of microplates between the major paleo-Eurasian and paleo-Afro-Arabian plates. The tectonic development of the region generally reflects the relative movements between the large plates, and the complications posed by the intervening microplates produced the puzzling geology in the Mediterranean region. The tectonic evolution of the Carpathian Mountains - Pannonian basin continues to present as evidenced by active seismicity to depths of ~200 km in the Vrancea region north of Bucharest (Stephenson et al., 1996).**

**During the Cenozoic, the Carpathian Arc evolved to assume its strongly arcuate shape (Csontos, 1995). This block experienced both rotations and translations. The subduction of oceanic areas between this block and paleo-Europe produced considerable Neogene volcanism. The resulting arc-related terranes were accreted to Paleozoic terranes to the north and east resulting in the formation of the Carpathian Fold and thrust belts. Back arc extension played the major role in the formation of the Pannonian Basin .**

## 2.2 Crust

**The Adriatic indenter, the Eastern Alps, the European Foreland and the Pannonian Basin differ significantly in their crustal structure. The crustal and lithopheric thickness of the European foreland ranges between 40 km to 50 km and 180 km to 200 km respectively. Thickening of the crust is observed in the region of the Tauern Window and Friuli, North East Italy, most likely related to isostasy. Beneath that domain the lithosphere forms a root reaching a depth of 220 km (Scarascia & Cassinis, 1997). In contrast, the crust and lithosphere of the Pannonian basin is thin and warm. Through intense Oligocene - Miocene stretching the crust was thinned out to 22 km to 30 km (Bada et al., 1999). A high heatflow causes a weak crust and is responsible for the loss of lithospheric strength. The heatflow pattern changed significantly from Oligocene to present times. In Miocene times extensional tectonics accompanied by the exhumation of large hot core complexes (e.g. Tauern Window, Ratschbacher et al. 1991, Neubauer et al., 2000) and magmatic activity especially within the Pannonian basin and along the Periadriatic Lineament caused elevated heatflow. The average present day heatflow of the European platform is around 60mW $m^{-2}$ . An average heatflow of 90 mW $m^{-2}$ makes the Pannonian crust and lithosphere weak in comparison to the cold and thick equivalents of the European Platform (Bada et al 1999).**

## 2.3 Stress

**The counter clockwise rotation of the Adriatic mircoplate around a pole at at 46.1°N 6.9°E with an angular velocity of 0.35 deg/Myr (Grenerczy et al., 2005) represents a**

**major source for tectonic stress within the Alpine-Pannonian region. The stress regime changed from Eocene to present times. Several stages of deformation pattern have been worked out for the northern Eastern Alps (Peresson and Decker, 1997), for the Southern Alps (Castellarin and Cantelli, 2000, Fellin et al., 2002), the Vienna and Danube basin (Fodor, 1995), the Pannonian basin and for the Western Carpathians The paleostress pattern from the domain of the Eastern Alps and the Pannonian basin are similar while the Southern Alps show significant differences.**

**The maximum horizontal stress (SH) orientation of the Western and Central European stress province rotates gradually from NW in the western parts to NE in the eastern parts, according to the Stress Map available at** www.world-stress-map.org **(Reinecker and Lenhardt, 1999).The Bohemian Massif shows a Central European stress pattern. This rigid block is flanked by units in the south and the east with a lower rheological strength. This rheology contrast is reflected by the radial stress pattern around the south Bohemian spur (Reinecker and Lenhardt, 1999; Bada et al., 1998). The stress trajectories are perpendicular to boundaries of high rheological contrast. The SH of the Bohemian basin and the Dinarides is NE oriented and therefore normal to the orogen (Gruenthal and Stromeyer, 1992).The stress pattern can be traced into the Pannonian basin (Horvath and Cloething, 1996). Within the basin the stress trajectories diverge. The western part of the Pannonian Basin belongs to the Western and Central European stress province. The orientation of SH in the eastern part of the Pannonian Basin is NNE to NE while the central Pannonian basin shows a SH orientation of WNW to NW.**

**The Eastern part of the Pannonian Basin represents a transition zone between the Western European stress province and the Dinarides stress province with predominantly E-W compression. The Adriatic stress province is characterized by north-south compression. SH progressively changes from NNE-SSW to ENE-WSW. These changes reflect the transition to the Pannonian-Dinaric stress province (Reinecker and Lenhardt, 1999).**

## 3. Overview of the CEGRN Campaigns and of the CERGOP-2 Data Base

**The CEGRN Network is intended to bridge the space between permanent GPS stations (distances 100-300 km) and national zero or first order networks (50-100 km). Measurements are usually made in June, to reduce seasonal effects which affect coordinates and, hence, velocities. Since 1997 the yearly campaigns have been replaced by campaigns every second year. Therefore the results presented here refer to campaigns in the years 1994, 1995, 1996, 1997, 1999, 2001, 2003 and 2005. The number of sites has grown from 30 to 90. Recently, the number of permanent stations is outweighing the number of epoch sites. A typical overview is seen in Fig. 2, presenting the last campaign CEGRN05. The RINEX files, ancillary files such as e.g. observation sheets and pictures, and an overview of the equipment used can be retrieved from the WEB page of the data center in Graz (OLG, 2006) .**


***Fig. 2 Map of GPS sites observed during the CEGRN05 campaign. Abbreviations and details of measurements can be seen at http://cergops2.iwf.oeaw.ac.at/CEGRN05info.html.***

**The database was set up on a dedicated WEB and FTP server (cergops2.oeaw.ac.at). A MySQL database provides the user with access information to the components of the CEGRN campaigns. For additional information, the website is linked to the CEGRN Consortium home page www.fomi.hu/cegrn, which maintains the station quality information and the administration affairs outside the EU project.**

## 4. Site validation and site specific issues

**A declared objective of the CERGOP-2/Environment project is the extension/densification of the CEGRN, while maintaining the high quality of the original network. Starting from 30 sites, in 2003 CEGRN has now 82 accepted sites which were approved by the site quality control group. According to the project's specifications for site selection (Fejes, 1993; Lévai et al., 1998), the site quality control group has inspected the monumentation and the antenna mount of most of the sites, has documented the horizon obscuration and checked the spectrum for unwanted radio emissions in the GNSS bands. Fortunately only a few CEGRN sites showed radio interference problems.**

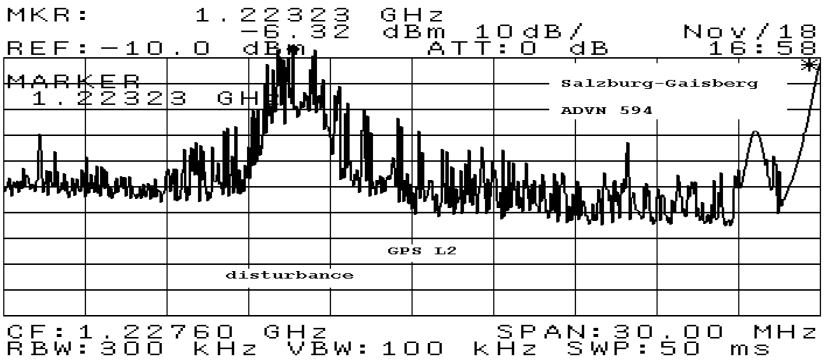


***Fig. 3 Radio spectrum surrounding the L2 frequency band at Salzburg - Gaisberg (SBGZ)***

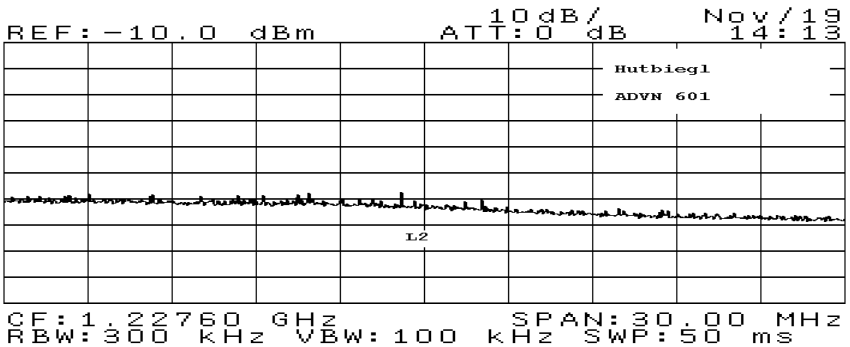


***Fig. 4 Radio spectrum surrounding the L2 frequency band at Hutbiegl (HUTB).***

**Fig. 3 gives an example of the radio spectra measured with an ADVANTEST spectrum analyser at Salzburg (SBGZ), Austria which is one of the problematic areas concerning radio interference environment. In comparison Fig. 4 shows a clean spectral environment at Hutbiegl (HUTB), Austria.**

**As a rule, we processed as nominal the sites found not compliant with the site validation criteria, but added a flag as a reminder, when evaluating or interpreting geokinematic results. Likewise, the outstanding site quality scored by stations such as GRAZ, HUTB, BRSK, GOPE, CSAR, DISZ, PENC, MATE, BOR1, GRYB, JOZE, LAMA and MOPI was considered as an element in the selections of sites to be used in the realization of a Central European reference frame.**

***Fig. 5. Example of changing multipath environment in CEGRN sites: a reference configuration is shown on the left. A test configuration with a metallic disk underneath the antenna is shown on the right.***

**In order to monitor data quality at a particular site specific issues on near field effects on the antenna (site multipath) and antenna calibration were addressed (Becker et al., 2004; Kirchner and Becker, 2004; Kirchner et al., 2004; Schönemann et al, 2006; Becker et al., 2006b).**

**Multipath behaviour can be described by periodical functions: the shorter the distance orthogonal to the reflecting surface, the longer the period of the multipath signature on phase, code and signal to noise (SNR) data (Elosegui et al., 1995; Bilich et al., 2004). The**

**long periodic multipath effects caused by reflectors in the near surrounding result in a constant or slowly varying bias in the coordinates which will not be averaged out. To understand the effect of changes in the multipath pattern in our typical measuring environment in more detail, we carried out a simple experiment. A LEIAX1202 antenna was mounted first on a pole (setup I, Fig. 5, left), to define a nominal setup. In a second phase, to generate a change in multipath environment, a steel pipe with a small disc on the top was put below the antenna (setup II, Fig. 5, right) in order to change the mounting without changing the antenna position and orientation. This simple modification in the mounting leads to a height jump of approximately 2.8 mm in the L2 solution and a much stronger effect (1-3 cm) in an ionosphere free solution with troposphere estimation. The horizontal position is less affected, below 1 mm in general. Experiments were conducted with different types of antennas, where the range of the effect varied between 0 to 3 mm in L2 (Schönemann et al., 2006; Becker et al., 2006a).**

| | dN [mm] | dE [mm] | dU [mm] |
|---|---|---|---|
| BZRG | -7.4 | -1.4 | 14.6 |
| BRAI | -7.4 | -1.4 | 13.4 |
| CLUJ | -7.4 | -1.4 | 15.6 |
| SIBI | -7.4 | -1.4 | 14.2 |
| SUCE | -7.4 | -1.2 | 14.6 |
| TIMI | -7.4 | -1.4 | 14.0 |

***Tab. 1 Differences in coordinates of CERGOP sites using LEIAT504 antennas, depending on the use of the pcv's appropriate to LEIAT504 vs. AOAD M_T antennas. Both are of the type choke ring with Dorne Margolin element.***

**The second specific issue we addressed is antenna calibration, which is important for the calibrations of phase center variations (pcv) as well as antenna gain corrections (Kirchner et al, 2004; Görres et al., 2006). As an example of the importance of a consistent use of the correct antenna calibration coefficients, a case study from the CEGRN network is shown. Due to lacking, in the first campaigns, of specific pcv's for the Leica LEIAT504 LEIS antenna (with radome), the original IGS values for the similar AOAD M_T Antenna were introduced. This antenna was used in a number of key stations during the CEGRN 2005 campaign. In the meantime the calibration table specifically computed for the LEIAT504 LEIS became available. The comparison between the two sets of pcv's used for this antenna led to differences in position and**

**height of about 7 and 14 mm respectively, see Table 1. Likewise, we find that ignoring or taking into account the radome causes differences of 2 to 5 mm in position and up to 9 mm in height, for the LEIAT504. The same holds for other types of antennas, where neglecting the radome leads to similar shifts in the coordinates. This example clearly implies that great care must be taken in the combination of campaign normal equations spanning several years, to ensure that pcv calibration consistency is maintained at all times.**

## 5. The CERGOP Velocities and Velocity Field in Central Europe

**Inputs to geokinematical modelling are epoch and permanent GPS long-term observations in the region of Central Europe, Eastern Alps, Dinarids and Balkan. The main information is expected from CERGOP epoch campaigns because of their relatively dense station distribution and long observing history. The permanent GPS stations in the region were also analyzed within the CERGOP-2/Environment and are used in combination with velocities derived from epoch observations to ensure that the realization of the Terrestrial Reference System resulting from this analysis is as rigorously as possible aligned and scaled to the state of the art International Terrestrial Reference Frame ITRF2000.**

**This section includes and extends the solution of six epochs of CEGRN GPS campaigns from 1994 to 2001 discussed by Stangl (2002), and the solution and combination of CEGRN in 2003 and 2005 given by Hefty et al. (2006). Network coordinates and their covariance matrices from all eight CEGRN epoch campaigns solutions are here used as input for velocity field evaluation.**

### 5.1 Epoch network analysis, combination and velocity field evaluation

**The epoch-wise observing campaigns of CEGRN comprising of five 24-hour simultaneous sessions have been performed since 1994. Initially, they were realised annually in years 1994, 1995, 1996, 1997, and then bi-annually in 1999, 2001, 2003 and 2005 in late spring.**

**The processing strategy was unique for all 8 epoch campaigns and obligatory for all Analysis Centres. Campaigns from 1994 to 2001 were reprocessed in 2002 with**

**improved models. The campaigns in 2003 and 2005 were processed just after their completion . The main features of computation strategy are: processing in daily intervals (0-24h UT), celestial reference frame realised by IGS orbits and corresponding Earth Rotation Parameters ( ERPs), 10º elevation cut-off, station zenith delays estimated at hourly intervals, Niell (1996) mapping function, and elevation dependent weighting. Models of phase center variations were consistent with IGS values. Selection of the baseline geometry and ambiguity resolution method was under the responsibility of individual analysis centres.**

**Results of separate processing of individual epoch campaigns after combination of outputs of at least two, up to five Analysis Centres were used to estimate the site coordinates and velocities, with time spans of up to 11 years.**

**The number of observed stations included in CEGRN was gradually increased. The first epoch campaign in 1994 included 23 stations. In 1995 the network comprises of 32 CEGRN stations (9 of them observed at that time already permanently) and included further 4 IGS reference stations to enable reliable referencing to ITRF. CERGOP 2005 campaign included 95 sites.**

**The characteristics of combined solutions of eight CEGRN observing campaigns are summarised in Tab. 2.**

| Observing campaign | Epoch of observation | No. of processed sites in the final solution | No. of solutions forming the network combination | RMS of unit weight for the combined solution (m) |
|---|---|---|---|---|
| CEGRN'94 | 1994.34 | 27 | 3 | 0.0023 |
| CEGRN'95 | 1995.41 | 36 | 3 | 0.0029 |
| CEGRN'96 | 1996.45 | 37 | 3 | 0.0030 |
| CEGRN'97 | 1997.43 | 45 | 4 | 0.0026 |
| CEGRN'99 | 1999.46 | 61 | 3 | 0.0024 |
| CEGRN'01 | 2001.47 | 55 | 2 | 0.0027 |
| CEGRN'03 | 2003.46 | 72 | 4 | 0.0024 |
| CEGRN'05 | 2005.47 | 95 | 5 | 0.0016 |

***Tab. 2. Main features of CEGRN campaigns analysed in this paper***

**In the last campaign in 2005 there were 18 sites for which the original monumentation from 1994 remained unchanged. These sites are promising the most reliable velocity estimation. There are 50 CEGRN non-reference sites where three or more epoch campaigns interval were performed at the identical position and the observing span is at**

**least three years. The network solution at each epoch resulted from the combination of the results of at least two independent analysis centers, so that sufficient redundancy was ensured. For velocity estimation we used the ADDNEQ2 program of the Bernese GPS software, version 5.0 (Hugentobler et al., 2004). The solution was validated by an independent velocity estimation model developed at the Slovak University of Technology using the error and weighting scheme described in this section (Hefty, 2004). The combination of CEGRN solutions from various epochs is referenced to ITRF2000 by constraining coordinates and velocities of set of selected IGS sites using their variances and covariances from the ITRF2000 solution (Boucher et al., 2004).**

**Results of individual CEGRN epoch campaigns (the combination of epoch solutions from individual analysis centres) are considered in the form of vector geocentric coordinates $\mathbf{X}_i$ and their covariance matrix $\Sigma_I$ (e.g. in the standard SINEX format). They refer to the epoch of observing campaign $t_i$. The coordinates of reference ITRF sites $\mathbf{X}_{ITRF}$ and velocities $\mathbf{v}_{ITRF}$ referred to epoch $t_0$ are considered as pseudo-observations. They are characterized by their covariance matrix composed from covariance matrices $\Sigma_{XITRF}$ , $\Sigma_{vITRF}$ and cross-covariance $\Sigma_{XvITRF}$ .**

**The estimated parameters are the geocentric coordinates of CEGRN sites. These are denoted as Y and the site velocities as $\mathbf{v}_Y$. Parameters Y and $\mathbf{v}_Y$. formally include also coordinates and velocities of reference sites. To align the CEGRN free-network solutions referred to epoch $t_i$ to the reference at epoch $t_0$, the 7-parameter spatial transformation with transformation parameters $\Theta_i$ has to be included into the model. Then the observation model relating observed values (results of CEGRN processing and ITRF coordinates and velocities) to estimated parameters (coordinates Y, velocities $\mathbf{v}_Y$ and transformation parameters $\Theta_i$ ) can be written in the form**

$$\begin{bmatrix} \mathbf{X}_1 \\ \mathbf{X}_2 \\ \vdots \\ \mathbf{X}_n \\ \mathbf{X}_{ITRF} \\ \mathbf{v}_{ITRF} \end{bmatrix} = \begin{bmatrix} \mathbf{A}_1 & \mathbf{D}_1 & \mathbf{T}_1 & \cdots & \mathbf{0} \\ \mathbf{A}_2 & \mathbf{D}_2 & \mathbf{0} & \cdots & \mathbf{0} \\ \vdots & \vdots & \vdots & \ddots & \vdots \\ \mathbf{A}_n & \mathbf{D}_n & \mathbf{0} & \cdots & \mathbf{T}_n \\ \mathbf{A}_{ITRF} & \mathbf{0} & \mathbf{0} & \cdots & \mathbf{0} \\ \mathbf{0} & \mathbf{D}_{ITRF} & \mathbf{0} & \cdots & \mathbf{0} \end{bmatrix} \begin{bmatrix} \mathbf{Y} \\ \mathbf{v}_Y \\ \Theta_1 \\ \vdots \\ \Theta_n \end{bmatrix} + \begin{bmatrix} \varepsilon_1 \\ \varepsilon_2 \\ \vdots \\ \varepsilon_n \\ \varepsilon_{XITRF} \\ \varepsilon_{vITRF} \end{bmatrix} \qquad \textbf{(5.1)}$$

**$\mathbf{A}_i$ design matrix relating observed coordinates with estimated coordinates (its elements are 1 or 0)**

| Site | campaigns | span (yr) | $v_X$ | $\sigma_{VX}$ | $v_Y$ | $\sigma_{VY}$ | $v_Z$ | $\sigma_{VZ}$ |
|---|---|---|---|---|---|---|---|---|
| BASO | 4 | 3 | -18.0 | 4.6 | 14.3 | 1.5 | 11.2 | 4.7 |
| LJUB | 8 | 11 | -16.5 | 1.1 | 16.6 | 0.4 | 11.0 | 1.2 |
| UPAD | 5 | 6 | -17.3 | 5.4 | 16.4 | 1.5 | 9.1 | 5.4 |
| BUCA | 6 | 10 | -13.5 | 2.3 | 20.0 | 1.1 | 10.2 | 2.5 |
| HARM | 4 | 9 | -18.2 | 1.9 | 18.0 | 0.9 | 5.3 | 2.0 |
| SOFI | 6 | 9 | -18.4 | 1.6 | 18.1 | 0.7 | 5.8 | 1.7 |
| BOR1 | 8 | 11 | -17.2 | 0.4 | 16.1 | 0.2 | 7.2 | 0.6 |
| JOZE | 8 | 11 | -17.8 | 1.0 | 16.2 | 0.4 | 7.7 | 1.4 |
| BRSK | 8 | 11 | -18.9 | 1.1 | 19.4 | 0.4 | 8.9 | 1.2 |
| MATE | 7 | 11 | -18.9 | 0.3 | 19.0 | 0.1 | 13.0 | 0.4 |
| DISZ | 8 | 11 | -18.4 | 1.1 | 19.5 | 0.4 | 6.5 | 1.3 |
| GILA | 4 | 4 | -31.2 | 4.5 | 11.0 | 2.0 | -8.5 | 5.1 |
| IAS3 | 3 | 4 | -28.8 | 4.0 | 11.7 | 2.1 | 0.5 | 4.8 |
| MACI | 3 | 3 | -24.7 | 4.1 | 14.6 | 2.2 | 3.9 | 4.7 |
| TIS3 | 5 | 9 | -12.2 | 1.8 | 18.4 | 0.8 | 15.3 | 1.9 |
| VAT1 | 3 | 3 | -17.3 | 12.9 | 17.1 | 6.3 | 8.9 | 15.3 |
| FUN3 | 4 | 6 | -6.8 | 3.6 | 21.4 | 1.8 | 14.1 | 4.0 |
| VRAN | 5 | 8 | -31.0 | 6.4 | 10.1 | 3.5 | -10.3 | 7.3 |
| GOPE | 8 | 11 | -16.2 | 0.9 | 17.5 | 0.3 | 8.5 | 1.1 |
| GRAZ | 8 | 11 | -17.6 | 0.3 | 18.0 | 0.1 | 8.1 | 0.4 |
| CSAR | 8 | 11 | -18.2 | 1.2 | 17.1 | 0.5 | 8.5 | 1.3 |
| GRMS | 4 | 4 | -15.7 | 8.1 | 21.8 | 2.4 | 11.6 | 8.9 |
| BOZI | 4 | 6 | -18.8 | 3.3 | 16.1 | 1.0 | 10.3 | 3.5 |
| BUCU | 4 | 6 | -18.2 | 2.9 | 16.6 | 1.5 | 5.4 | 3.1 |
| BZRG | 4 | 6 | -15.7 | 3.5 | 16.9 | 1.0 | 7.9 | 3.7 |
| CSAN | 4 | 6 | -18.0 | 3.5 | 17.2 | 1.6 | 8.1 | 3.8 |
| DRES | 4 | 6 | -12.0 | 2.3 | 17.3 | 0.8 | 15.5 | 2.8 |
| DUBR | 3 | 4 | -22.1 | 5.8 | 14.7 | 2.3 | 7.3 | 5.6 |
| HVAR | 5 | 8 | -24.6 | 1.8 | 18.8 | 0.6 | 7.1 | 1.7 |
| KAME | 4 | 6 | -18.6 | 3.1 | 16.4 | 1.3 | 6.8 | 3.7 |
| LYSA | 4 | 6 | -16.2 | 2.7 | 17.1 | 1.2 | 9.8 | 3.2 |
| MALJ | 4 | 6 | -19.9 | 3.5 | 16.6 | 1.1 | 8.5 | 3.6 |
| PART | 4 | 6 | -19.2 | 2.7 | 15.1 | 1.1 | 10.0 | 3.1 |
| POL1 | 4 | 6 | -14.2 | 2.8 | 14.9 | 1.0 | 11.9 | 3.4 |
| SBGZ | 4 | 6 | -14.1 | 2.4 | 18.3 | 0.8 | 11.9 | 2.6 |
| SRJV | 4 | 6 | -18.0 | 4.0 | 17.4 | 1.5 | 9.5 | 4.0 |
| SULP | 5 | 8 | -17.6 | 1.7 | 16.0 | 0.8 | 8.6 | 2.2 |
| TARP | 4 | 6 | -18.6 | 3.3 | 15.5 | 1.5 | 6.7 | 3.8 |
| TUBO | 5 | 10 | -15.8 | 2.6 | 17.4 | 1.0 | 10.3 | 3.0 |
| WROC | 4 | 6 | -16.2 | 2.2 | 15.8 | 0.9 | 8.8 | 2.8 |
| MEDI | 4 | 6 | -18.6 | 3.7 | 18.1 | 1.1 | 9.3 | 3.7 |
| HUTB | 8 | 11 | -17.9 | 2.0 | 18.2 | 0.7 | 8.4 | 2.4 |
| MOPI | 8 | 11 | -14.9 | 1.0 | 17.3 | 0.4 | 10.7 | 1.2 |
| PENC | 8 | 11 | -18.7 | 0.9 | 17.1 | 0.3 | 6.7 | 1.0 |
| WTZR | 6 | 9 | -15.8 | 0.2 | 17.1 | 0.1 | 8.6 | 0.4 |
| GRYB | 8 | 11 | -18.4 | 1.1 | 16.0 | 0.4 | 7.2 | 1.3 |
| LVIV | 7 | 10 | -17.0 | 1.4 | 15.9 | 0.6 | 8.8 | 1.8 |
| SKPL | 8 | 11 | -16.4 | 1.2 | 16.8 | 0.5 | 8.1 | 1.5 |
| UZHD | 8 | 11 | -18.2 | 1.1 | 16.3 | 0.5 | 7.1 | 1.4 |
| HOHE | 7 | 11 | -13.9 | 1.1 | 16.7 | 0.3 | 12.9 | 1.2 |
| HFLK | 6 | 10 | -14.0 | 1.7 | 18.1 | 0.5 | 10.5 | 1.8 |
| LAMA | 8 | 11 | -18.8 | 1.0 | 13.8 | 0.4 | 4.7 | 1.4 |
| METS | 8 | 11 | -16.0 | 0.3 | 14.8 | 0.2 | 8.6 | 0.6 |
| STHO | 8 | 11 | -18.3 | 1.3 | 17.4 | 0.5 | 7.7 | 1.5 |
| SNIE | 8 | 11 | -14.0 | 1.0 | 14.9 | 0.4 | 5.9 | 1.3 |
| POTS | 7 | 10 | -16.2 | 1.0 | 16.2 | 0.3 | 7.7 | 1.3 |
| KIRS | 5 | 5 | -17.3 | 3.0 | 16.6 | 1.0 | 8.0 | 3.8 |
| KOSG | 8 | 11 | -13.5 | 0.3 | 16.6 | 0.1 | 9.7 | 0.5 |
| ONSA | 8 | 11 | -13.6 | 0.2 | 14.8 | 0.1 | 9.4 | 0.4 |
| ZIMM | 8 | 11 | -14.0 | 0.4 | 18.6 | 0.2 | 9.9 | 0.5 |
| UNPG | 3 | 4 | -16.2 | 2.2 | 15.8 | 0.9 | 8.8 | 2.8 |

***Tab. 3. Velocities of CEGRN sites observed three or more epochs expressed in geocentric coordinate system, number of campaigns, time span covered by epoch campaigns. Reference frame is ITRF2000. Velocities and their uncertainties are in mm/year.***

| Site | $v_X$ | $\sigma_{VX}$ | $v_Y$ | $\sigma_{VY}$ | $v_Z$ | $\sigma_{VZ}$ |
|---|---|---|---|---|---|---|
| BASO | 3.6 | 1.1 | -2.8 | 1.0 | -1.9 | 6.6 |
| LJUB | 1.9 | 0.3 | -0.8 | 0.3 | -0.3 | 1.6 |
| UPAD | 1.6 | 1.3 | -1.1 | 1.0 | -3.1 | 7.6 |
| BUCA | -3.2 | 0.6 | 0.6 | 0.5 | 4.7 | 3.5 |
| HARM | -3.2 | 0.5 | 0.4 | 0.4 | -2.8 | 2.8 |
| SOFI | -2.3 | 0.5 | 0.7 | 0.4 | -3.2 | 2.4 |
| BOR1 | -0.3 | 0.2 | 0.6 | 0.2 | -1.6 | 0.7 |
| JOZE | -0.2 | 0.3 | 0.8 | 0.3 | -0.6 | 1.7 |
| BRSK | 1.4 | 0.3 | 2.4 | 0.2 | -2.8 | 1.6 |
| MATE | 4.1 | 0.2 | 1.1 | 0.1 | -1.2 | 0.4 |
| DISZ | -0.9 | 0.4 | 2.8 | 0.3 | -3.3 | 1.7 |
| GILA | -1.3 | 1.2 | -0.0 | 0.9 | -23.0 | 6.9 |
| IAS3 | 2.5 | 1.0 | 0.7 | 0.8 | -13.3 | 6.4 |
| MACI | 0.8 | 1.1 | 1.0 | 0.8 | -7.7 | 6.5 |
| TIS3 | 0.4 | 0.5 | -1.0 | 0.4 | 8.0 | 2.7 |
| VAT1 | -0.8 | 2.4 | 0.3 | 1.7 | 0.9 | 20.8 |
| FUN3 | -5.2 | 1.0 | -0.7 | 0.8 | 12.1 | 5.5 |
| VRAN | -3.2 | 2.1 | -0.2 | 1.6 | -23.6 | 10.0 |
| GOPE | -0.1 | 0.3 | 0.9 | 0.2 | -0.8 | 1.4 |
| GRAZ | 0.4 | 0.2 | 1.1 | 0.1 | -2.4 | 0.4 |
| CSAR | 0.7 | 0.4 | 0.3 | 0.3 | -2.2 | 1.8 |
| GRMS | 1.0 | 1.9 | 4.3 | 1.4 | 1.4 | 12.0 |
| BOZI | 3.3 | 0.9 | -0.7 | 0.7 | -2.7 | 4.8 |
| BUCU | -2.6 | 0.8 | -0.4 | 0.6 | -2.7 | 4.3 |
| BZRG | -0.3 | 0.9 | -0.6 | 0.7 | -2.6 | 5.0 |
| CSAN | -0.1 | 1.0 | 0.5 | 0.9 | -1.7 | 5.3 |
| DRES | 1.3 | 0.8 | 0.1 | 0.6 | 7.3 | 3.6 |
| DUBR | 2.7 | 1.7 | -1.5 | 1.3 | -7.2 | 8.1 |
| HVAR | 3.7 | 0.5 | 3.0 | 0.4 | -8.6 | 2.5 |
| KAME | -0.5 | 0.9 | 0.5 | 0.7 | -2.2 | 4.9 |
| LYSA | 0.1 | 0.9 | 0.5 | 0.8 | 1.0 | 4.2 |
| MALJ | 2.7 | 0.9 | -0.2 | 0.7 | -4.8 | 5.0 |
| PART | 2.9 | 0.9 | -0.7 | 0.6 | -1.5 | 4.1 |
| POL1 | 0.9 | 0.9 | -2.0 | 0.7 | 3.0 | 4.3 |
| SBGZ | 0.7 | 0.8 | 0.7 | 0.6 | 2.3 | 3.5 |
| SRJV | 1.0 | 1.0 | 0.1 | 0.8 | -1.8 | 5.7 |
| SULP | -0.2 | 0.5 | -0.0 | 0.4 | 0.4 | 2.8 |
| TARP | -0.4 | 0.9 | -0.5 | 0.7 | -2.5 | 5.1 |
| TUBO | 0.5 | 0.9 | 0.6 | 0.6 | 1.1 | 4.0 |
| WROC | 0.1 | 0.8 | -0.4 | 0.6 | 0.0 | 3.5 |
| MEDI | 2.3 | 1.0 | 0.6 | 0.7 | -3.9 | 5.2 |
| HUTB | 0.7 | 0.6 | 1.7 | 0.5 | -1.9 | 3.1 |
| MOPI | -0.0 | 0.3 | -0.0 | 0.2 | 1.9 | 1.6 |
| PENC | -0.3 | 0.3 | 0.9 | 0.2 | -3.1 | 1.4 |
| WTZR | 0.0 | 0.1 | 0.3 | 0.1 | -1.1 | 0.4 |
| GRYB | -0.1 | 0.3 | 0.2 | 0.3 | -2.0 | 1.7 |
| LVIV | -0.5 | 0.4 | -0.3 | 0.3 | 0.9 | 2.3 |
| SKPL | -1.0 | 0.4 | 0.1 | 0.3 | -0.2 | 1.9 |
| UZHD | -0.6 | 0.4 | 0.2 | 0.3 | -1.7 | 1.8 |
| HOHE | 1.9 | 0.3 | -0.9 | 0.2 | 2.5 | 1.6 |
| HFLK | 0.0 | 0.5 | 0.4 | 0.4 | 0.8 | 2.4 |
| LAMA | -0.4 | 0.3 | -0.6 | 0.3 | -3.7 | 1.7 |
| METS | -1.4 | 0.2 | 1.0 | 0.2 | 3.2 | 0.7 |
| STHO | 0.0 | 0.4 | 1.1 | 0.3 | -2.0 | 2.0 |
| SNIE | -3.1 | 0.4 | -1.9 | 0.3 | -1.5 | 1.7 |
| POTS | 0.0 | 0.3 | 0.4 | 0.3 | -1.3 | 1.6 |
| KIRS | 0.7 | 0.8 | 0.7 | 0.6 | -1.7 | 4.9 |
| KOSG | 0.3 | 0.2 | 0.2 | 0.1 | 0.4 | 0.6 |
| ONSA | -0.8 | 0.1 | -0.1 | 0.1 | 2.4 | 0.4 |
| ZIMM | 0.4 | 0.2 | 0.7 | 0.2 | -0.7 | 0.6 |
| UNPG | -2.1 | 1.7 | -2.0 | 1.4 | -5.4 | 9.5 |

***Tab. 4. Velocities of CEGRN sites observed more than 3 epochs evaluated in reference frame ITRF2000 reduced for APKIM model and expressed in local coordinate system. Units are mm/yr.***

**$A_{ITRF}$ design matrix relating ITRF coordinates with estimated coordinates (its elements are 1 or 0)**

**$\mathbf{D}_i$** **design matrix relating observed coordinates with estimated velocities (its elements are $t_i - t_0$ or 0)**

**$\mathbf{D}_{ITRF}$** **design matrix relating ITRF velocities with estimated velocities (its elements are 1 or 0).**

**$\mathbf{T}_i$** **design matrix for transformation of epoch campaigns to ITRF**

**$\mathbf{Y}$** **coordinate parameters: coordinates of epoch sites as well as of reference sites**

**$\mathbf{v}_Y$** **velocity parameters: velocities of epoch sites as well as velocities of reference sites**

**$\Theta_i$** **transformation parameters from *i*-th epoch $t_i$ to reference epoch $t_0$**

**$\boldsymbol{\varepsilon}$** **vectors of errors of observed quantities**

***n*** **number of epoch campaigns**

**Stochastic properties of observed quantities can be characterized by global covariance matrix**

$$\mathrm{var}\begin{pmatrix} \mathbf{X}_1 \\ \mathbf{X}_2 \\ \vdots \\ \mathbf{X}_n \\ \mathbf{X}_{ITRF} \\ \mathbf{v}_{ITRF} \end{pmatrix} = \begin{bmatrix} \vartheta\boldsymbol{\Sigma}_1 & \mathbf{0} & \cdots & \mathbf{0} & \mathbf{0} & \mathbf{0} \\ \mathbf{0} & \vartheta\boldsymbol{\Sigma}_2 & \cdots & \mathbf{0} & \mathbf{0} & \mathbf{0} \\ \vdots & \vdots & \ddots & \vdots & \vdots & \vdots \\ \mathbf{0} & \mathbf{0} & \cdots & \vartheta\boldsymbol{\Sigma}_n & \mathbf{0} & \mathbf{0} \\ \mathbf{0} & \mathbf{0} & \cdots & \mathbf{0} & \boldsymbol{\Sigma}_{XITRF} & \boldsymbol{\Sigma}_{XvITRF} \\ \mathbf{0} & \mathbf{0} & \cdots & \mathbf{0} & \boldsymbol{\Sigma}^T_{XvITRF} & \boldsymbol{\Sigma}_{vITRF} \end{bmatrix} \qquad \textbf{(5.2)}$$

**where $\vartheta$ is the variance factor scaling the covariance matrices from epoch solutions $\Sigma_i$ to be consistent with reference ITRF coordinates and velocities. The observations in various epochs $t_i$ are considered as mutually independent. Estimation of parameters – coordinates, velocities and transformation parameters and their covariance matrix is based on standard least-squares approach (Koch, 1999).**

**Setting of the coordinate and velocity parameters in eq. 5.1 was restricted to sites measured at least three epochs. The ITRF2000 coordinates and velocities of 8 IGS stations with their covariance matrix at the epoch 1997.0 were extracted from the ITRF2000 SINEX file and used for frame definition. The selection of the reference sites was determined by the requirement that their velocities are obtained from combination of two space techniques at least (GPS and VLBI and/or SLR). This criterion is met by the IGS stations BOR1, GRAZ, KOSG, MATE, WTZR, ONSA and ZIMM, which were included in CEGRN epoch campaign processing. Velocities at 52 non-reference sites**

**were then determined on the basis of 1014 coordinate observations included in vectors $X_i$ on the left-hand side of (5.1). The variance factor $\vartheta$ was determined iteratively by fulfilling the criterion to obtain the a posteriori variance of unit weight close to one. The final solution was obtained with $\vartheta$ = 53. This factor scales the uncertainties from CEGRN campaign solutions (which are usually overestimated) with the uncertainties of coordinates and velocities of ITRF2000 extracted from the ITRF2000 covariance matrix. The estimated CEGRN velocities and their uncertainties expressed in geocentric reference system are summarized in Tab. 3. We stress that the coordinates of reference sites are also formally estimated, however setting the factor $\vartheta$ in covariance matrix (5.2) guarantees that the estimated coordinates of reference sites are differing from ITRF values only minimally. Residuals exceeding 2 cm in one of the coordinates were treated as outliers and eliminated.**

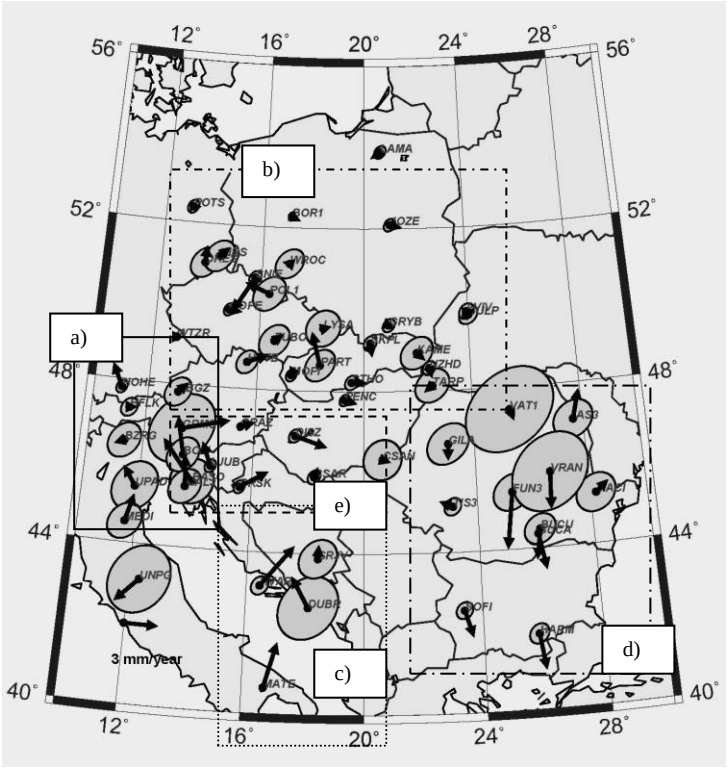


***Fig. 6 Intraplate horizontal velocities with 2σ error ellipses, obtained from CEGRN velocities by removing the corresponding APKIM 2000 velocities. The following provinces are identified from kinematics: a) Adria Indenter, b) Central Europe, c) Dinaric compression,d) Downward migration of Eastern Carpathians (?), e) Lateral extrusion to the Pannonian Basin.***

**The uncertainties are depending mainly on time span of observations (sites with longest observation history cover 11 years), then on number of used campaigns (from 3 to 8) and on quality and repeatability of site epoch observations.**

**To obtain information about an intraplate velocity field, model velocities were removed from the estimated velocities. We used two global plate motions models:**

- **The NNR-NUVEL 1A geophysical plate motion model (DeMets et al., 1994) based on paleomagnetic data, earthquake slip vector data etc.**
- **The APKIM 2000 (Drewes, 1998) plate motion model using the VLBI, SLR and GPS observations.**

**The root mean square error of the two sets of horizontal intraplate velocities (when the NUVEL model or APKIM model was applied) indicates, as it can be expected that the APKIM is yielding smaller residual velocities. While the Nuvel model is based mostly on data from ocean floor spreading, the APKIM model is based on geodetic velocities on the continental shelf including the central part of Europe. It is worth to mention that the strain rates inferred from the symmetric part of the intraplate velocity gradient will be minimally influenced by the choice of model reducing the global motion, which is based on rigid rotation, and hence on the antisymmetric part of the velocity gradient.**

**The resulting intraplate velocities (with the APKIM model velocities removed) and their RMS errors are summarized in Tab. 4. Visualisation of intraplate horizontal velocities are in Fig. 6. Their uncertainties are represented by $2\sigma$ error ellipses.**

**The CEGRN intraplate horizontal velocities fall roughly into three regional groups:**

- **A Central European part (about 30 CEGRN sites) has velocities with small amplitudes, generally up to 1 mm/year and random orientation. Amplitudes on sites with observation history longer than 8 years only slightly exceed their $2\sigma$ error ellipses. The only station in the region with long (11-year) observing history and a significant velocity (4 mm/year) is SNIE. It is very probable that this is a local phenomenon, although our site quality control group reports no evidence of instability. The other two stations with shorter observing history which do not meet the general behaviour of this part of network are POL1 and PART. Stations within, or near the Pannonian Basin have velocities about 2 mm/year generally oriented to east (GRAZ, HUTB, DISZ, PENC, STHO, KAME).**

- **Stations close to the Adriatic region have velocities directed to north and northeast (MEDI, MALJ, BOZI, LJUB, BRSK, HVAR, DUBR, SRJV). Their magnitudes range, with the exception of HVAR, from 2 to 4 mm/year and the velocity vectors are exceeding the $2\sigma$ confidence. Unfortunately the observation history of majority of them is shorter than 8 years.**
- **Balkan stations situated in Bulgaria (SOFI, HARM) and some stations Romania (MACI, BUCU, BUCA) with velocities oriented to south and southeast. Magnitude of the velocities is from 2 to 4 mm/year and all the vectors are exceeding the $2\sigma$ intervals. However note, that the orientation of other Romanian stations (MACI, IAS3, TIS3) is not uniform with this general trend.**

**The vertical velocities $v_h$ are not influenced by removal of velocities resulting from a rigid rotation model. The magnitudes of vertical velocities are above $1\sigma$ level only occasionally. Vertical velocities differing from zero by more than $1\sigma$ are reported for POTS, LAMA, VRAN, IAS3, HVAR and are very probably of local nature (Fig. 7).**

**The relevance of estimated horizontal velocities obtained from CEGRN epoch observations is now examined by comparison with independently computed velocities of permanent GPS observations. We will use three sources of information:**

- **ITRF2000 velocity field, epoch 1997 (Boucher et al., 2004), reduced for APKIM 2000.**
- **European permanent network station velocities expressed in ETRF 2000, epoch 1997 (Kenyeres, 2006).**
- **Velocities inferred from 3-year interval of permanent observations in Central Europe region (Hefty and Igondová, 2006).**

**For those CEGRN stations such that the three kinds of velocities previously mentioned are available we find that there is generally good agreement between the compared velocities. The uncertainty of epoch CEGRN velocities is generally larger than those derived from permanent observations. This is obvious consequence of significantly smaller number of observations at epoch sites when compared to number of observations at permanent sites even the time span covered by epoch observations is usually longer. The comparison of ITRF2000 and EUREF estimates with our values of the velocities of permanent common stations suggests that epoch observations can**

**provide valuable results for sites where no permanent observations are available, provided the total time span is sufficiently large and proper care is given to the alignment of the reference system.**

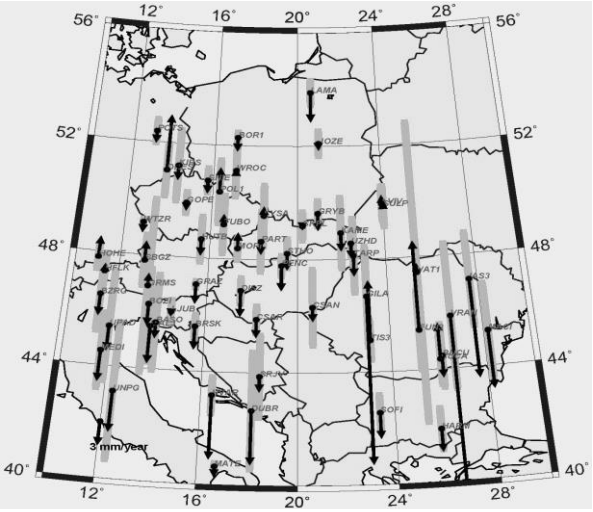


*Fig. 7 Vertical velocities obtained from CEGRN analysis, and their $2\sigma$*

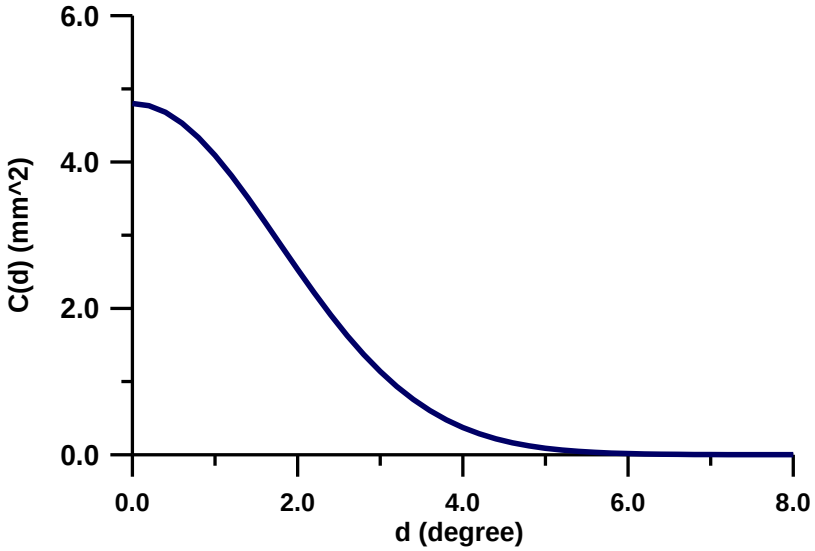


*Fig. 8 Covariance function of signal used for interpolation of CEGRN velocity field*

## 5.2 Velocity field in a regular grid

**As is evident from Fig. 6 the distribution of sites with known velocities is not uniform and also remarkable are the differences in uncertainties of velocities at individual sites. To obtain the information suitable for geo-kinematical modelling and subsequently for strain analysis we will firstly interpolate the discrete velocities to a regular grid. Grid spacing must be defined consistently with the data distribution and the uncertainty of**

**the interpolated velocities must also be examined carefully, especially in areas of less dense population of stations.**

**For horizontal velocity interpolation we use Least Squares Collocation (Moritz, 1973), where the two-dimensional signal part is represented by horizontal components of intraplate velocities. The covariance of the velocities can be approximated by a function *C*(*d*)**

$$C(d) = \sigma_{0s}^2 \exp\left(-c^2 d^2\right) \qquad \textbf{(5.3)}$$

**where *d* is spherical distance between the measured and interpolated points expressed in degrees, $\sigma_{0s}$ is the variance of the velocities and *c* is the scale distance for decorrelation of velocity pairs.**

**Best fit to the variogram of the velocities yields $\sigma_{0s} = 2$ mm/yr and *c* = 0.35 deg$^{-1}$. The graphical representation of the used covariance function is in Fig. 8. The characteristic distance of decorrelation of approximately 300 km agrees with earlier independent estimates in the Alpine Mediterranean area (Caporali et al., 2003), suggesting that this is a measure of the average flexural wavelength of the lithosphere.**

**Application of least squares collocation method to interpolation of horizontal velocities $\mathbf{v}_{pred}$ is based on simple relation (Moritz, 1973)**

$$\mathbf{v}_{pred} = \mathbf{C}_S \mathbf{C}_v^{-1} \mathbf{v}_{obs} \qquad \textbf{(5.4)}$$

**where $C_S$ is covariance matrix of signal, and $v_{obs}$ is the vector of CERGN velocities reduced for APKIM and for a mean value and $C_v$ is their covariance matrix. The mean velocity is restored after interpolation. The covariance matrix of signal is set up from elements defined according to eq. 5.3.**

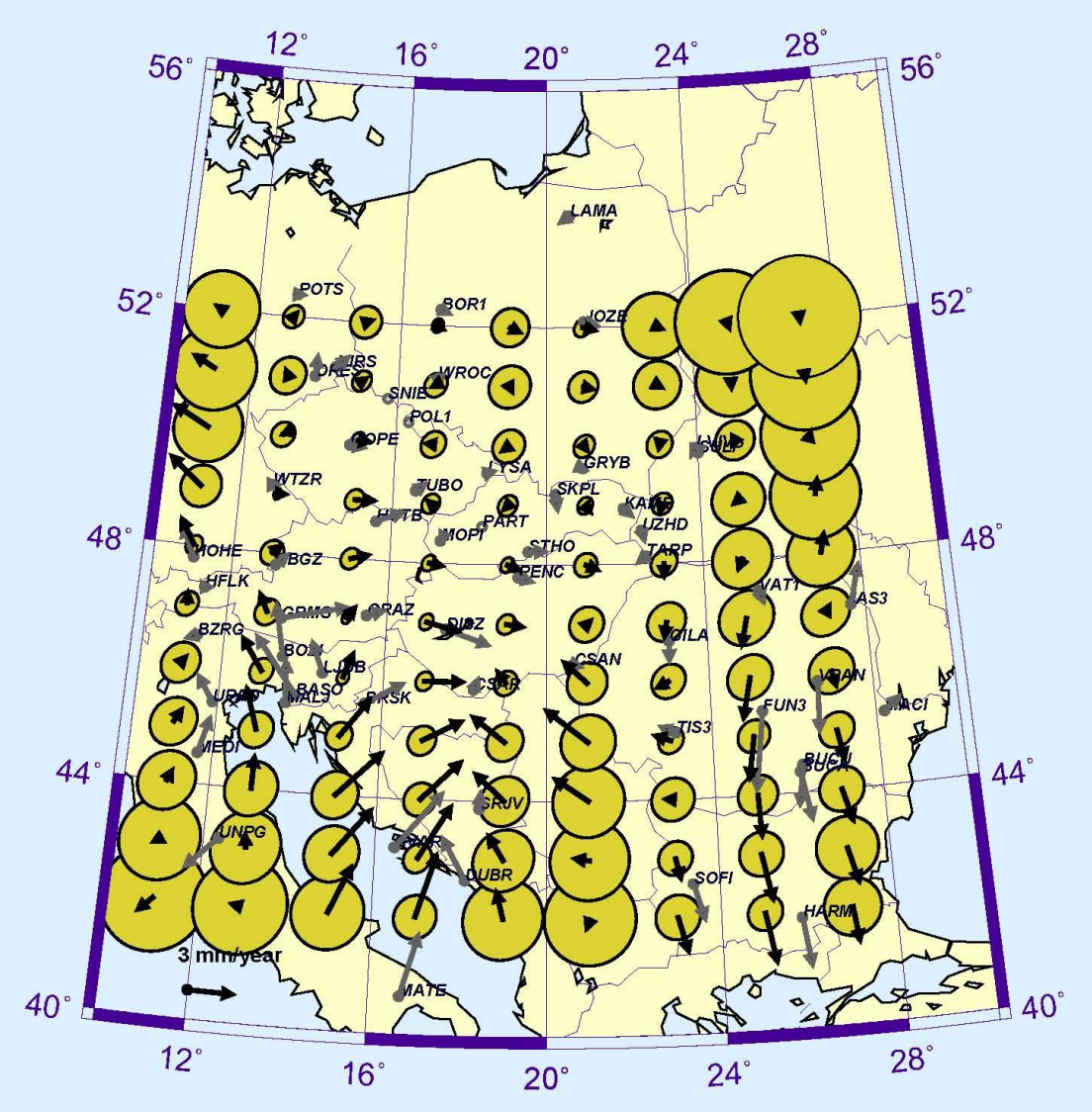


***Fig. 9 Interpolation of CEGRN horizontal velocities into 2º x 1º grid (black vectors with one-sigma error ellipses). The gray vectors show the observed CEGRN velocities.***

**The geographical distribution of sites with CEGRN velocities as well as their uncertainties are inhomogeneous, so the optimum choice of grid for interpolated velocities is not trivial and the statistical reasons are not strictly defined. We choose a 2º**

**x 1° grid, as a compromise between data density and spatial resolutions, over most of the study area.**

**Fig. 9 shows the interpolation on the 2° x 1° grid, where the original velocities are also plotted. Note that the interpolation procedure respects the uncertainties and stochastic relation among the observed velocity field.**

**The main characteristics of the interpolated CERGOP intraplate horizontal field can be summarised as:**

- **About 1 mm/year motions in northern part of Central Europe at the limit of 2-sigma confidence.**
- **1-2 mm/year differently oriented motions in central part of Central Europe exceeding 2-sigma confidence**
- **North-west oriented velocities in Adriatic region and Central Balkan up to 4 mm/year.**

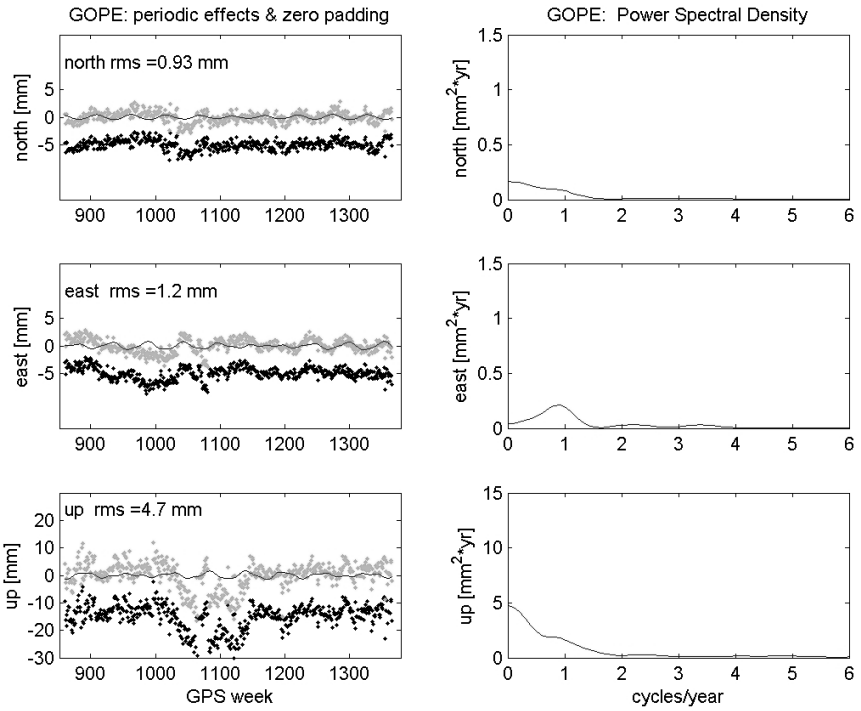


**Fig. 10:** ***Detrended time series of GOPE and identification and removal of periodic signatures from the series. Left, the time series with outliers removed are superimposed with an empirical sinusoid with 6, 12 and 14 month periods (continuous curve). The time series below, with a bias of -5 mm for plotting purposes, represents the unbiased time series with the overlaying sinusoid (black continuous curve) removed. Missing data are replaced with zeros. Right, Power Spectral Density of the unfiltered time series, highlighting the dominating frequency bands.***

- **South oriented velocities in east Balkan about 3 mm/year generally exceeding 2-sigma limits.**
- **Regions at the borders of maps in Fig. 9. where the velocities are mainly extrapolated and have uncertainties significantly exceeding their magnitudes.**

## 6. Characterization of the noise of permanent GPS stations used for the realization of ITRF2000

**The time series of station coordinates need to be carefully analysed, especially if the stations have been observed throughout the history of the project, and are to be used in the realization of the Reference Frame ITRF2000. Examples of such stations are GOPE, JOZE and PENC. These are also part of the European Permanent Network and continuous time series of their coordinates can be computed over a time period of 10 years, since 1996.**

**The procedure we have developed to address the analysis of time series is based on i) a validation of the time series with respect to sudden jumps or discontinuities which can invalidate the local velocity and the realization of the reference frame, and hence affect all the other stations, and ii) on a detailed time and frequency analysis which quantifies the noise and the stability of the series.**

**For those stations free of discontinuities and with time series longer than three years, such as GOPE, for example, we proceed as follows: first we estimate and subtract 6,12 and 14 month sinusoids (see example in Fig. 10); secondly we compute PSD (Power Spectral Density) and spectral index of each coordinate, to understand the amount and type of non white noise, and the autocorrelation function (see example in Fig. 11);Finally we compute the Allan variance, as a measure of the stability of the series (i.e. probability of a change in slope) (see example in Fig. 12).**

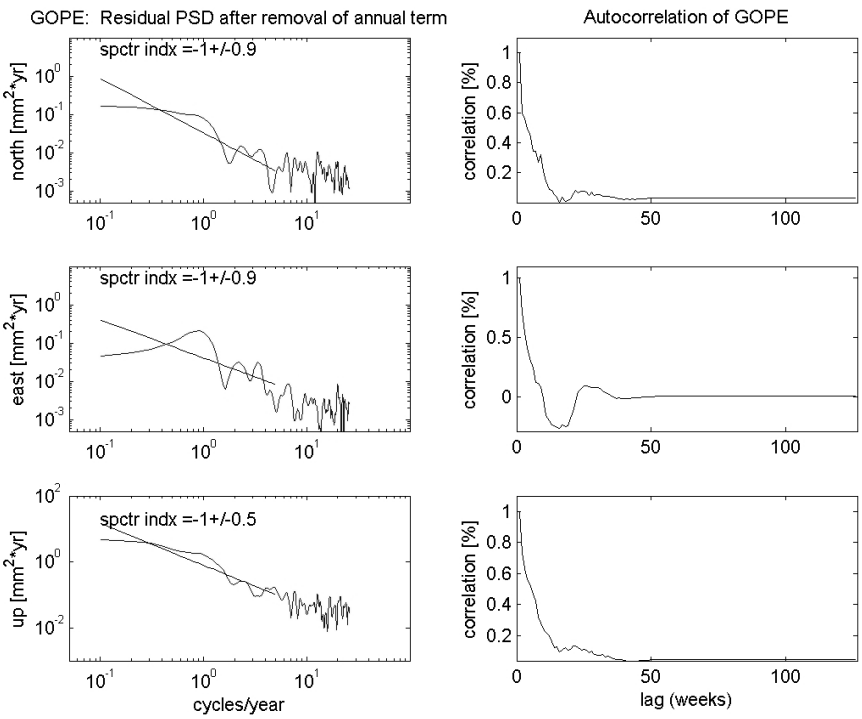


***Fig. 11 : Left the Power Spectral Density of time series with sinusoids removed plotted on a loglog scale exhibit colored noise at low (< 2 cycles/year) frequencies and white noise at higher frequencies. The low frequency PSD can be interpolated with a straight line and its slope (typically negative or zero) is classified according to Table 5. Right, the autocorrelation function is a measure of how statistically independent the samples entering the time series are. Analysis programs such as ADDNEQ normally assume the autocorrelation function to be a Dirac delta. Our analysis shows that this is not exactly true, but that the effects in the numerical value of the slope –or velocity- due to the autocorrelation of the data are in most cases negligibly small.***

$$S_x(f) \approx G_x(f) = \sum_{i=0}^{4} \frac{k_{-i}}{f^i} \quad \left[ mm^2 yr \right]$$

i = 0 White Noise of Position;
i = 1 Flicker Noise of Position;
i = 2 White Noise of Velocity
or Random Walk of Position;
i = 3 Flicker Noise of Velocity;
i = 4 Random Walk of Velocity

**Tab. 5. The low frequency part of a power law PSD can be approximated, in a loglog space, with a straight line, whose slope is the spectral index. The spectral index defines the type of white or colored noise. The computation of the spectral index is exemplified in Fig. 11.**

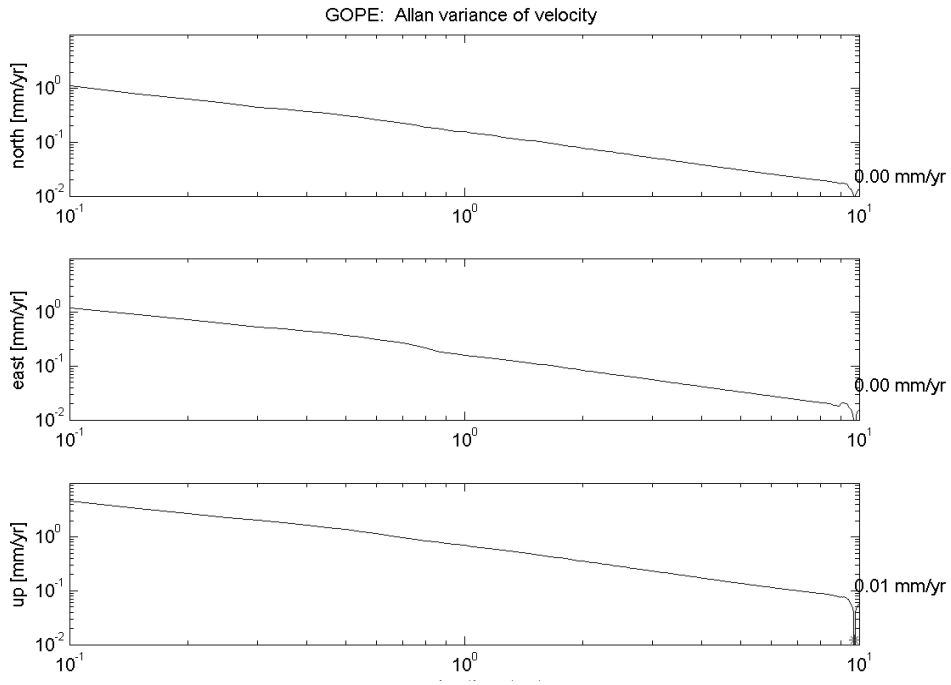


***Fig. 12. The Allan variance of a time series is a measure of its stability, i.e. the maximum change in slope to occur with 1 σ probability from one batch of data of length T, the averaging time, to a contiguous, non overlapping and equal length batch of data. In the case of GOPE the estimated square root of the Allan variance of the horizontal components of velocity fall below .01 mm/yr, which is not exceptional for extremely stable time series of long (ca. 10 yr) duration.***

**The detailed algorithms are discussed by Caporali (2003) and the systematic analysis is reported in the web page http://cisas.unipd.it/gps/project.html. Overall the stations with the longest time series show a horizontal repeatability below 1 mm r.m.s. and a stability, in the sense of Allan variance, better than 0.1 mm/yr. This justifies the expectation that the inferred kinematics of the investigated area is properly defined in a geodetic sense, both spatially and temporally.**

## 7. Strain analysis

**The velocity field in regular grid serves as the input for the calculation of strain parameters. According to theoretical background given e.g. by Altiner (1999) or Cai**

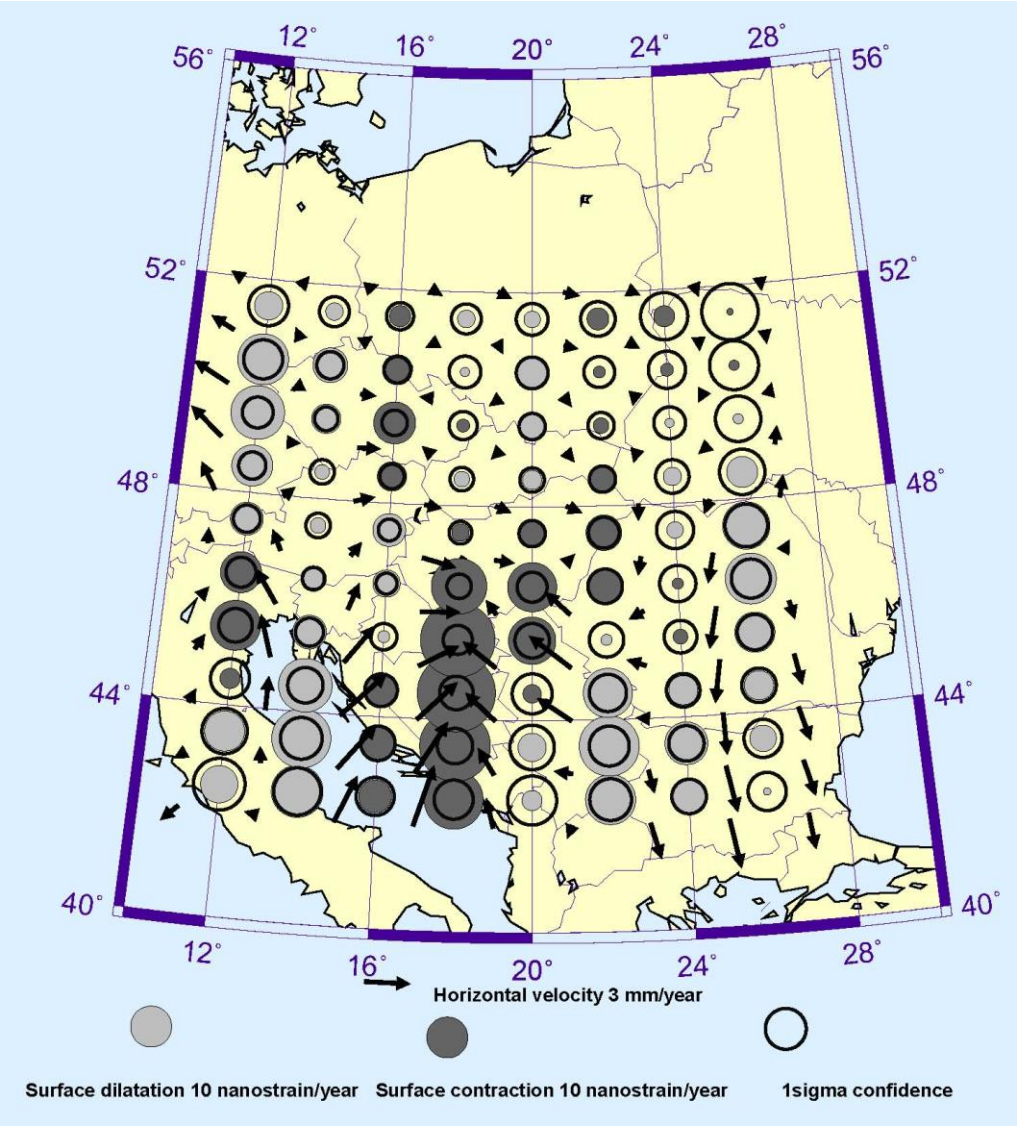


***Fig. 13 Surface dilatation and surface contraction $\theta$. Magnitudes of $\theta$ and their one-sigma confidence intervals are proportional to the area of circles.***

**(2004) we evaluated from horizontal velocities components $v_n$ and $v_e$ the main strain parameters, namely:**

- **Surface dilatation or depression $\theta$**
- **Shear constituents and maximum shear strain $\gamma$**
- **Principal strain rates $\varepsilon_1$, $\varepsilon_2$ (eigenspace components) and their orientation angle $\alpha$.**

**We present strain estimates averaged on spherical elementary rectangles of size 2º x 1º . To this purpose one has first to compute the elements of velocity gradient tensor**

$\frac{\partial v_n}{\partial n}, \frac{\partial v_n}{\partial e}, \frac{\partial v_e}{\partial n}, \frac{\partial v_e}{\partial e}$ **averaged over the elementary rectangle. Then the derived quantities** $\theta$**,** $\gamma$**,** $\varepsilon_1$**,** $\varepsilon_2$ **and** $\alpha$ **can be computed (Caporali et al., 2003). The uncertainties of all parameters are derived from uncertainties of interpolated velocities using the propagation of variance-covariance law. Generally, n stations at an average distance of 200 km and average uncertainty in the velocity of 1 mm/year will define a strain rate value with an uncertainty of the order of** $5n^{1/2}$ **nstrain/year (1 nanostrain =** $10^{-9}$**). Hence we can expect a 2 sigma typical significance level of the order of 15 to 20 nanostrain/year.**

**The surface isotropic dilatation** $\theta = \frac{\partial v_n}{\partial n} + \frac{\partial v_e}{\partial e}$ **, (if** $\theta > 0$**) or contraction (if** $\theta < 0$**) are shown in Fig. 13. If we take into account the uncertainties of** $\theta$**, several regions with large** $\theta$ **are dominating:**

- **Surface contraction in the central part of the Balkans and in the Pannonian basin with magnitude from 20 up to 40 nanostrain/year. This is the most pronounced compression region in the investigated area.**
- **Surface dilatation in the east Balkan with magnitude from 10 to 20 nanostrain/year, however the observed** $\theta$ **are only slightly exceeding their one-sigma confidence.**
- **Surface dilatation area in the north Adriatic region with magnitudes at the level of their one-sigma confidence.**
- **Surface dilatation in the north-west part of the monitored territory with magnitude from 5 to 15 nanostrain/year.**

**The central part of monitored area is characteristic with moderate** $\theta$ **(up to 10 nanostrain/year)**

**The magnitude of shear strain is shown in Fig. 14. It is evident that shear strain is dominant in almost all the monitored region – majority of the values in rectangular grid**

**are over one-sigma interval, in some rectangles the magnitude is significant at the 5 sigma level.**

**The principal axes of strain rates $\varepsilon_1$ and $\varepsilon_2$ are shown in Fig. 15. This figure is the geodetic counterpart 0f a World Stress Map (Reinecker et al., 2005) based on geophysical data.**

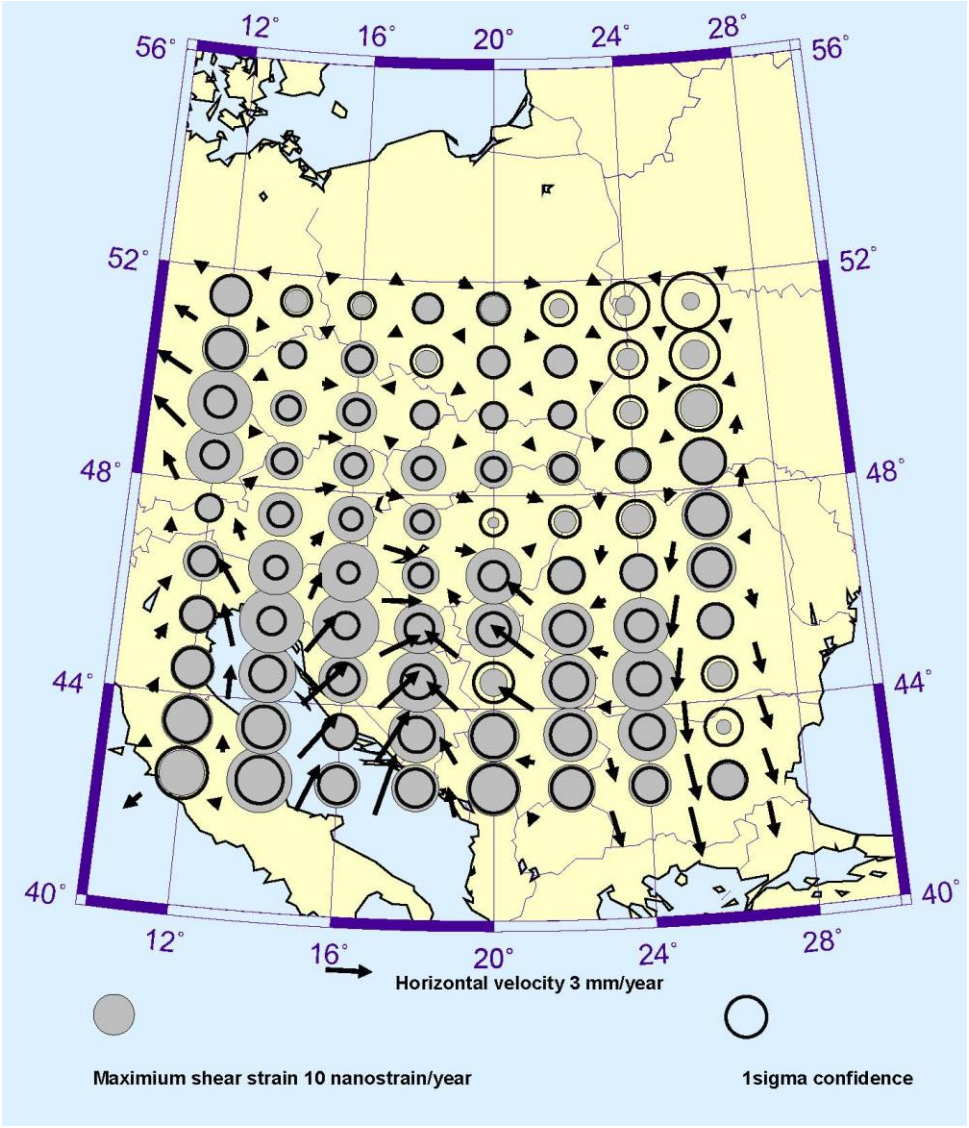


*Fig. 14 Surface shear strain magnitudes and their uncertainties*

## 8. Discussion

**The following paragraphs summarizes the major tectonic constraints found during the CERGOP-I and II projects based on the results presented in the previous sections 5, 6 and 7 and further integrated analyses published earlier by Becker et al, (2002), Caporali**

**et al., (2003), Grenerczy et al., (2000), and (2005), Hefty et al, (2004), and Hefty, (2005) in the framework of these projects.**

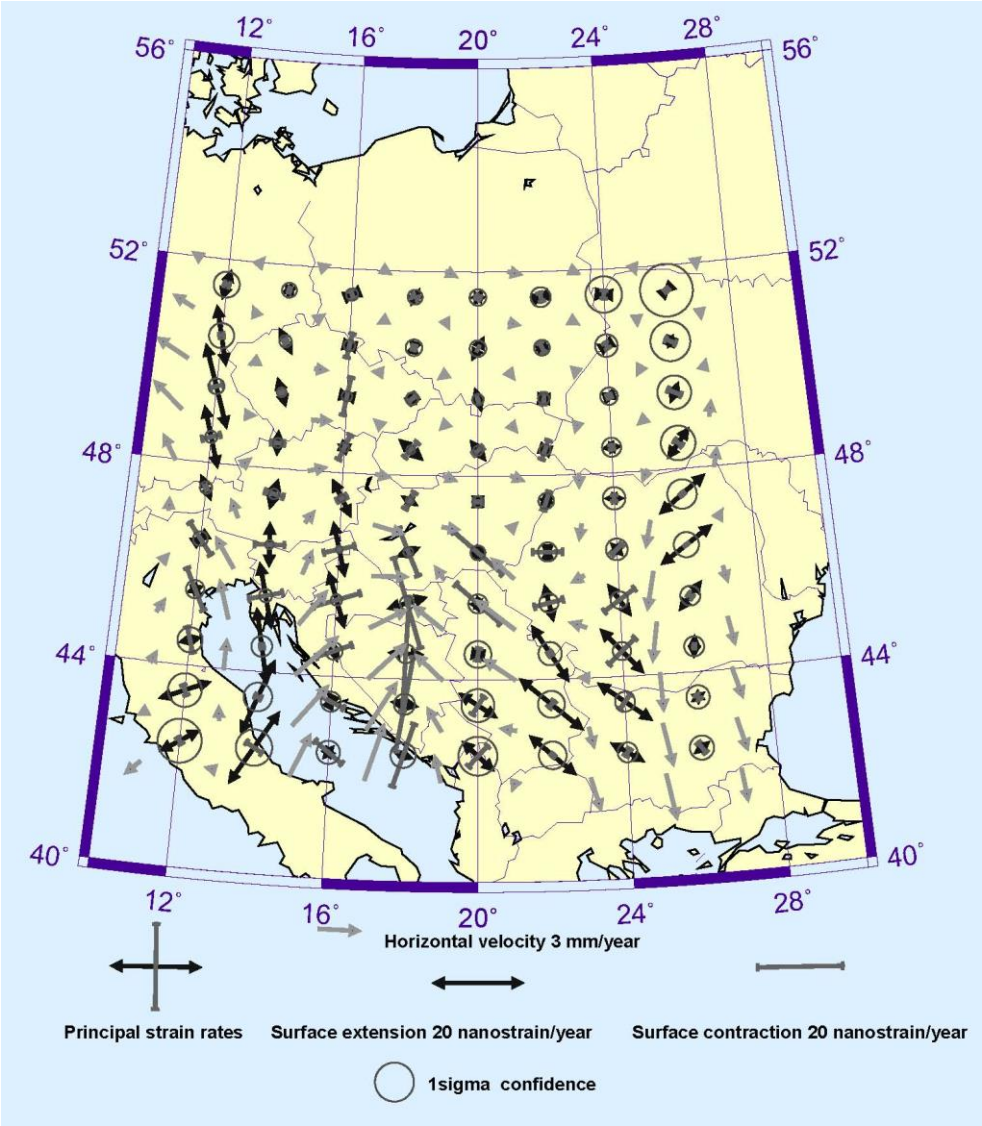


*Fig. 15. Principal rates $\varepsilon_1$ and $\varepsilon_2$, their orientation and their one-sigma confidence*

## 8.1 European Platform

**The European Platform in a present-day kinematic definition consists of all tectonic domains located north of the Alps and the Carpathian Arc regardless whether the domain is Precambrian, affected by the Caledonian orogeny, or the later Hercynian orogeny. The CEGRN data show that the majority of active contraction originating from the Eurasia Nubia plate boundary and the microplate between them is taken up either in the Alps, the Dinarides, and the Pannonian Basin. No significant deformation is visible at or near the Carpathian Arc. After the calculation of the Euler motion for**

**stable Europe from these data, the residual velocities have random orientations with 0.3 mm/yr scatter.This low figure provides an upper estimate for the level of rigidity of the European Platform.**

## 8.2 Adria microplate

**Adria microplate is the most active, fastest moving, major tectonic stress source that dominantly shapes the deformation of South Central Europe (Pinter et al., 2006). Independence of Adria from Nubia and Eurasia were tested and proved, F-ratio tests were performed (Stein and Gordon, 1984) for several subsets of sites believed to be on Adria and the two plate model assumption (Adria-Eurasia) turned out to be valid for all of the tests, its motion and boundaries were also outlined and suggested its possible fragmentation (Grenerczy et al., 2005). Based on Euler vector calculation and seismicity, it seems that the microplate is fragmenting along the Gargano-Dubrovnik seismic zone. The Euler pole and angular velocity calculated for the Po-Plain, Northern Adria, and the whole Adria microplate were compared to earlier estimates of Anderson and Jackson, (1984), Ward, (1994), Calais et al., (2002), and Battaglia et al., (2004). The strain distribution along at the Italian part was further analyzed by Caporali et al., (2003) and the extensional strain across the Appenines was also determined (Hefty, 2005).**

## 8.3 Eastern Alps

**A 2.3 mm/yr north-south oriented convergence rate is implied by our data between Adria and the Southern Alps, and a narrow -~60 km wide- contraction zone in the Southern Alps is identified, consistently with earlier results (Grenerczy et al., 2005), (D'Agostino et al., 2005) (Caporali et al., 2006). The Adria block appears as a wedge intruding into the southern part of the Eastern Alps. The velocity magnitudes abruptly drop below 0.5 mm/yr in the Southern Alps, leaving the majority of the Alps free of significant present-day contraction. ~30 nanostrain/yr contraction rate in the Southern Alps was observed and eastward extrusion north of the contraction zone was detected (Grenerczy et al., 2000), which corresponds with the extension found at the Tauern Window by Caporali et al, (2006). The seismicity and focal mechanisms are in good agreement with this present-day tectonic scenario suggested by the GPS data.**

## 8.4 Central Dinarides

**In the southeastern boundary of the microplate 4-4.5 mm/yr motion of Adria decreases to ~1 mm/yr through the microplate, its boundary, and the Dinarides mountain range towards the southwestern part of the Pannonian Basin. After a 1.5 mm/yr -probably- abrupt change at the boundary, the velocity magnitudes decrease slowly and gradually across a far wider zone in the Central Dinarides than in the case of the Eastern Alps. The uniform contraction rate from the Adriatic coast to the Pannonian basin is 6-7 nanostrain/yr, which is equivalent with around 2 mm/yr shortening within approximately 360 km. At the Central Dinarides the tectonic style seems different. The thin, weak lithosphere of the Pannonian Basin is located E of the N-S compression in the Eastern Alps, eastward extrusion and strike-slip deformation contribute to taking up the deformation there. However, because the basin is behind the Central Dinarides rather than to their side and there is no rigid block like the European Platform north of the Alps, no lateral extrusion occurs (Grenerczy et al., 2005). Therefore the contraction is much less intense in the case of the Central Dinarides and the contraction zone is more than five times larger. A much more detailed study can be given in a couple of years as we have been measuring more than 20 Bosnian GPS sites (Mulic et al., 2006) and a few additional sites in Serbia.**

### 8.5 Pannonian Basin

**Our data suggest that if the Pannonian Basin is subject to deformation, then it is most likely to be compressional than extensional. We performed a baseline length time series analysis, based on HGRN (Hungarian Geodynamic Reference Network), CEGRN, and EPN (European Permanent Network) data. More than 40 GPS vectors (baselines) were processed and the time series of the change of their distances were analyzed. Linear regressions, statistical tests were performed and we determined the contraction rate within the Pannonian Basin with its confidence limits. This additional check yielded a 1.5 ± 0.5 mm/yr contraction. Shortening was observed across the whole basin in N-E direction in the northern part and NE-SW direction in the southern part of the Pannonian Basin (Grenerczy and Kenyeres, 2006). This contraction can be seen on Fig. 15.**

## 8.6 Carpathian Arc

**During Miocene times, subduction and volcanism were gradually extinguished along the Carpathian arc from west to east and then to south. The migration of the young Carpathian orogenic belt was limited by the edge of the European Platform (Horváth, 1993). A slab can now only be detected at the southeastern bend of the Carpathian arc at the Vrancea zone (Oncescu, 1984) where the present-day deformation is being investigated by dense local GPS surveys. (Dinter et al., 2001, Van der Hoeven et al., 2003). The CEGRN network has several sites in the region operating since 1995, but the relocations of those sites and the extent and density of this regional network do not allow us to surpass these detailed studies there.. Our GPS data show that compression and associated contraction due to the Adria collision with the Alps and the Dinarides are not taken up in the mountain belts and the contraction can be detected far over the collisional boundaries. The Eastern Alps, the Dinarides, and further to the northeast, the Pannonian Basin all act as the compressional stress absorbers and almost entirely take up the energy of the collision. GPS velocities and strain calculation show no significant deformation to the north-northeast in the Western and Northern Carpathians (Fig. 9). If the source of seismicity in the Vrancea zone is at depth, for example connected to the sink of a lithospheric slab into the mantle, then we expect that more detailed surveys will confirm the small horizontal deformation we have measured by GPS. Vertical deformation or mass deficits detected by levelling and respectively gravimetric campaigns could help in validating the model.….**

## Acknowledgements

**Particular thanks are due to Dr. Peter Pesec, who coordinated the CERGOP-2/Enviromental project among 14 participating institutions and provided scientific and financial reports in due times for Brussels. This work was supported by the EU EVK2-CT-2002-00140 grant. The Hungarian team acknowledges the support of OTKA T042900 and MŰI TP 108 grants.**

## References

**Altiner, Y., 1999. Analytical Surface Deformation Theory. Berlin - Heidelberg, Springer Verlag. 102 pp.**

**Anderson, H., Jackson, J., 1987. Active tectonics of the Adriatic region, Geophys. J. R. astr. Soc., 91, 937-983.**

**Bada, G., Cloetingh, S. A. P. L., Gerner, P., Horváth, F., 1998. Sources of recent tectonic stress in the Pannonian region: inferences from finite element modelling, Geophys. J. Int., 134, 87–102.**

**Barlik M., Borza T., Busics I., Fejes I., Pachelski W., Rogowski J., Sledzinski J., Zielinski J., 1994. Central Europe Regional Geodynamics Project. Reports on Geodesy No.2(10), 7-24.**

**Becker, M., E. Cristea, M. Figurski, L. Gerhatova, G. Grenerczy, J. Hefty, A. Kenyeres, T. Liwosz, G. Stangl, 2002. Central European intraplate velocities from CEGRN campaigns, Reports on Geodesy., l(61), 83-91.**

**Becker, M., Kirchner, M., P. Zeimetz, 2004. Site and equipment calibration for GPS observation facilities in the CERGOP-2/Environment project. Proceedings 3rd CERGOP-2 Conference, Sofia, Sept. 30- Oct., 2004, Reports on Geodesy, Warsaw University of Technology, ISSN 0867-3179, No. 4 (71), 23-34, Warsaw.**

**Becker M., Caporali A., Figursky, M., Grenerczy, Gy., Kenyeres, A., Hefty, J., Marjanovic, M., Stangl, G., 2002. A Regional ITRF Densification by Blending Permanent and Campaign Data - The CEGRN campaigns and the Central European Velocity Field. Vistas for Geodesy in the New Millennium, eds. J. Ádám, K.-P. Schwarz, International Association of Geodesy Symposia, Vol. 125, pp. 53-58, Springer-Verlag, Berlin-Heidelberg-New York.**

**Becker, M., Schönemann, E., Zeimetz, P. 2006a. Gelöste und ungelöste Probleme der Antennenkalibrierung, GPS und GALILEO – Methoden, Lösungen und neueste Entwicklungen, Schriftenreihe des DVW, Band 49, Wißner Verlag, 189–210, ISBN 3-89639-521-1.**

**Becker, M., Drescher, R., Schönemann, E., Gutwald, J. 2006b. Improvements in CEGRN station monitoring and in the CEGRN velocity field. Proceedings of final CERGOP-2 Working Meeting, Graz, Austria, July 13. - 14., Reports on Geodesy No. 3 (78) , in press.**

**Bilich, A., Larson, K. M., Axelrad, P., 2004. Observations of signal-to-noise ratios (SNR) at geodetic GPS site CASA: Implications for phase multipath, Proceedings of the Centre for European Geodynamics and Seismology, 23, 77-83.**

**Boucher, C., Altamimi, Z., Sillard, P., Feissel-Vernier, M., 2004. The ITRF 2000. IERS Technical note No. 31. Fankfurt am Main, Verlag des Bundesamtes für kartographie und Geodäsie.**

**Cai, J., 2004. Statistical Inference of the Eigenspace Components of a Symmetric Random deformation tensor. Deut. Geod. Komm. Reihe C, Heft Nr. 577 131 pp.**

**Calais, E., Nocquet, J.M., Jouanne, F., Tardy, M., 2002.Current strain regime in the Western Alps from continuous GPS measurements, 1996-2001, Geology, 30-7, 651-654.**

**Caporali, A., 2003. Average strain rate in the Italian crust inferred from a permanent GPS network - I.Statistical analysis of the time-series of permanent GPS stations. Geophysical Journal International, 155, 241-253 ISSN: 0956-540X.**

**Caporali A., Martin S, Massironi M., 2003. Average strain rate in the Italian crust inferred froma a permanent GPS network - II.Strain rate vs. Seismicity and Structural Geology. Geophysical Journal International, 155, 254-268 ISSN: 0956-540X.**

**Caporali A., Massironi, M., Nardo, A., 2006. Constraining the seismic budget of Adria indentation and the dynamics of fault interaction with geodetic strain rate data, paper presented at Wegener 2006 meeting, Sept., 2006, Nice, France.**

**Castellarin, A., Cantelli, L., Fesce, A.M., Mercier, J.L., Picotti, V., Pini, G.A., Prosser, G., Selli, L., 1992. Alpine compressional tectonics in the Southern Alps. Relationships with the N-Apennines. Annales Tectonicæ, VI (1), 62-94.**

**Csontos, L., 1995. Tertiary tectonic evolution of the Intra-Carpathian area: a review, Acta Vulcanologica, 7(2) 1–13.**

**DeMets, C., Gordon, R. G., Argus, D. F., Stein, S., 1994. Effect of recent revisions to the geomagnetic reversal time scale on estimates of current plate motions. Geophys. Res. Lett. 21, 2191 – 2194.**

**Dinter, G., Nutto, M., Schmitt, G., Schmidt, U., Ghitau, D., Marcu, C., 2001. Three dimensional deformation analysis with respect to plate kinematics in Romania, Reports on Geodesy, 2(57): 29-42.**

**Drewes, H., 1998. Combination of VLBI, SLR and GPS determined station velocities for actual plate kinematics and crustal deformation models. In: Forsberg, R., Feissel, M., Dietrich, R. (eds.): Geodesy on the Move, Gravity, Geoid, Geodynamics, and Antarctica, IAG Symposia Vol. 119, Springer, pp. 377-382.**

**Elosegui, P., Davis, J. L., Jaldehag, R. K., Johansson, J. M., Niell, A. E., Shapiro, I. I., 1995. Geodesy using the global positioning system: The effects of signal scattering on estimates of site position. J. of Geophys. Res., 100:9921–9934.**

**Fellin, S., Martin, S., Massironi, M., 2002. Polyphase tertiary fault kinematics and Quaternary reactivation in the Central-Eastern Alps (Western Trentino). Journal of Geodynamics 34, 31-46.**

**Fejes I., 1993. The GRL hierarchy of the GPS Reference Frame. Proc. IRIS'93 Workshop "Reference Frame Establishment and Technical Developments in Space Geodesy", pp.181-186. Ed. T. Yoshino, Communication Research Laboratory, Tokyo, Japan.**

**Fejes I., 2006. Consortium for Central European GPS Geodynamic Reference Network (CEGRN Consortium). In The Adria Microplate: GPS Geodesy, Tectonics, and Hazards, eds. N. Pinter, G. Grenerczy, J. Weber, S. Stein, D. Medak, Springer, Dordrecht, 183-194.**

**Fodor, L., 1995. From transpression to transtension: Oligocene-Miocene structural evolution of the Vienna Basin and the East Alpine – Western Carpathian junction, Tectonophysics, 242, 151–182.**

**Ge L., Han S., Rizos C., 2002. GPS multipath change detection in permanent GPS stations, Survey Review, 36(283), 306-322.**

**Görres, B., Campbell, J., Becker, M., Siemes, M., 2006. Absolute Calibration of GPS Antennas: Laboratory results and comparison with field and robot techniques. GPS Solutions, 10, 2006, 136-145.**

**Grenerczy, Gy., Kenyeres, A., Fejes, I., 2000. Present crustal movement and strain distribution in Central Europe inferred from GPS measurements, J. of Geophys. Res. 105B9, 21,835-21,846.**

**Grenerczy, Gy., Sella, G., Stein, S., Kenyeres , A., 2005. Tectonic implications of the GPS velocity field in the northern Adriatic region, Geophys. Res. Lett., 32, L16311, doi:10.1029/2005GL022947.**

**Grenerczy, Gy., Kenyeres, A., 2006. GPS velocity field from Adria to the European Platform, in The Adria Microplate: GPS Geodesy, Tectonics, and Hazards, Editors: N. Pinter, G. Grenerczy, D. Medak, S. Stein, and J. C. Weber, Springer, Dordrecht, pp. 321-334.**

**Gruenthal, G., Stromeyer, D., 1992. The recent crustal stress field in Central Europe: Trajectories and finite element modeling. J. of Geophys. Res. 97, NO. B8, 11,805–11,820.**

**Hefty, J., Igondovà, M., 2006. Geokinematical implications inferred from analysis of permanent stations in Central Europe region. Proc. of EGU General Assembly Symposium G6,Vienna, 2006. Reports on Geodesy (in print).**

**Hefty, J.: 2006. Work-package 7 of the CERGOP-2/Environment: GPS data analysis and the definition of reference frame. Final report: April 2003 – July 2006. Reports on Geodesy (in print) .**

**Hefty J., Gerhátová L., Igondová M., Kováè M., Hrèka M., 2004. The Network of Permanent GPS Stations in Central Europe as the Reference for CERGOP Related Activities, Reports on Geodesy No. 2. (69) 115-123.**

**Hefty J., 2005. Kinematics of Central European GPS Geodynamic Reference Network as the Result of Epoch Campaigns During Nine Years, Reports on Geodesy No. 2. (73), 23-32 .**

**Hoeven van der, A.G.A., Ambrosius, B.A.C., Spakman, W., Mocanu, V., 2003. Crustal motions in the Eastern Carpathians (Vrancea) measured by GPS, Geophysical Research Abstracts, 5: 03918.**

**Horv´ath, F. Cloetingh, S. A. P. L., 1996. Stress-induced late-stage subsidence anomalies in the Pannonian basin, Tectonophysics, 266, 287–300.**

**Hugentobler, U., Dach, R. and Fridez, P. (eds) 2004. Bernese GPS software, Version 5.0. Draft. Bern: Astronomical Institute, University of Berne.**

**Koch, K.R., 1999. Parameter estimation and hypotheses testing in linear models. Heidelberg, Springer, 333 pp.**

**Jolivet, L., and Faccenna, C., 2000. Mediterranean extension and the Africa-Eurasia collision: Tectonics, 19, 1095–1106.**

**Kenyeeres, A., 2006. EPN Project Time series for geokinematics. Product available at www.epncb.oma.be.**

**Kirchner, M., Becker, M.: Design of New Permanent Observation Facilities for the CERGOP-2/Environment Project. In: Reports on Geodesy Vol. 69, No. 2, pp. 25-31, Proceedings of the EGU Symposium G11 "Geodetic and Geodynamic Programmes of the CEI (Central European Initiative)". Nice, France, April 25.-30.**

**Kirchner, M., Becker, M., Häfele, P., 2004. Calibration and Validation of New GPS Observation Equipment for the CERGOP-2/Environment Project. In: Reports on Geodesy Vol. 69, No. 2, pp. 271-284, Proceedings of the EGU Symposium G11 "Geodetic and Geodynamic Programmes of the CEI (Central European Initiative)". Nice, France, April 25.-30.**

**Kirchner M., Becker M., 2005, The use of signal strength measurements for quality assessment of GPS observations, Reports on Geodesy No. 2 (73), 245-253.**

**Lévai P., Borza T., Fejes I., Kujawa L., Mojzes M., 1998, CERGOP Study Group No. 2: Site Quality Monitoring. (Final Report). Reports on Geodesy No.10 (40), 114-167.**

**Mulic M., Bilajbegovic, A., Altiner, Y., 2006. Study of the effects of processing strategy variations on GPS position estimates, Geophysical Research Abstracts, Vol. 8, 04734, European Geosciences Union.**

**Neubauer, F., Fritz, H., Genser, J., Kurz, W., Nemes, F., Wallbrecher, E., Wang, X., Willingshofer, E., 2000. Structural evolution within an extruding wedge: model and application to the Alpine-Pannonian system, in: Urai, J., Lehner, F., and van Zee, W. (Eds.): Aspects of tectonic faulting (Festschrift in Honour of Georg Mandl), Springer, 141–153.**

**Niell, A.E., 1996. Global mapping functions for the atmosphere delay at radio wavelengths, J. of Geophys. Res. 101B2, 3227-3246.**

**OLG, 2006: CEGRN Data Center Graz, http://cergops2.iwf.oeaw.ac.at/CEGprojresult.html**

**Oncescu, M.C., 1984. Deep structure of the Vrancea region, Romania, inferred from simultaneous inversion for hypocenters and 3-D velocity structure, Annales Geophysicae, 2, 23-28.**

**Peresson, H. Decker, K., 1997. The Tertiary dynamics of the northern Eastern Alps (Austria); changing palaeostresses in a collisional plate boundary, Tectonophysics, 272, 125–157.**

**Pinter, N., Gy. Grenerczy, D. Medak, S. Stein, and J. C. Weber (Editors), 2006.The Adria Microplate: GPS Geodesy, Tectonics, and Hazards, Springer, Dordrecht, 1-413.**

**Ratschbacher, L., Frisch, W., Linzer, H.-G., Merle, O., 1991. Lateral extrusion in the Eastern Alps, part 2. Structural analysis, Tectonics, 10, 257–271.**

**Reinecker, J. and Lenhard, W. A., 1999. Present-day stress field and deformation in eastern Austria, Int. Jour. Earth Sci., 88, 532– 550.**

**Reinecker, J., Heidbach, O., Tingay, M., Sperner, B., Müller, B., 2005. The release 2005 of the World Stress Map (available online at www.world-stress-map.org).**

**Scarascia, R., Cassinis, R., 1997. Crustal structures in the central- eastern Alpine sector: a revision of the available DSS data. Tectonophysics, 271, 157-188.**

**Schönemann, E., Becker, M., 2005: GPS Antenna Calibration and Site Dependent Behaviour, Proceedings of 6th CERGOP-2 Working Conference and CEGRN**

**Consortium Meeting, Sarajevo, Bosnia-Herzegovina, November 9-10, 2005, Reports on Geodesy, No. 4, (75), 33-46.**

**Schönemann, E., Becker, M., J. Gutwald, J. , 2006: A software module for quality control of CEGRN site. Proceedings of the EGU Symposium G6 "Geodetic and Geodynamic Programmes of the CEI (Central European Initiative)". Vienna, Austria, April 2.-4. 2006, Reports on Geodesy No. 1 (76), 1-8.**

**Stangl, G., 2002. Creating a common CEGRN solution. The rules behind. Reports on geodesy No. 1 (61), 23-25.**

**Stein, S., Gordon, R., 1984. Statistical tests of additional plate boundaries from plate motion inversions, EPSL, 69, 401-412.**

**Stephenson, R.A., Wilson, M., de Boorder, H., Starostenko, V., 1996. EUROPROBE Intraplate Tectonics and Basin Dynamics of the Eastern European Platform - Preface, Tectonophysics, 268, i-iv.**

**Ward, S., 1994. Constraints on the seismotectonics of the central Mediterranean from Very Long Baseline Interferometry, Geophys. J. Int., 11, 441-452.**